Geochemistry, Geophysics, Geosystems

RESEARCH ARTICLE
10.1029/2019GC008239

Genesis and Architecture of Sequences of Quaternary Coral Reef Terraces: Insights From Numerical Models

A.-M. Pastier[1,2,3], L. Husson[1], K. Pedoja[4], A. Bézos[3], C. Authemayou[5], C. Arias-Ruiz[3], and S. Y. Cahyarini[6]

[1]ISTerre, CNRS, Université Grenoble Alpes, Grenoble, France, [2]M2C, CNRS, Université de Rouen, Rouen, France, [3]LPG Nantes, CNRS, Université Nantes, Nantes, France, [4]Normandie Univ, Unicaen, Unirouen, CNRS, M2C 1400, Caen, France, [5]Univ Brest, CNRS, UMR 6538 (Laboratoire Geosciences Ocean), Institut Universitaire Europeen de la Mer (IUEM) , Place Nicolas Copernic, 29280 Plouzané, France, [6]Research Center for Geotechnology, Indonesian Institute of Sciences, LIPI, Bandung, Indonesia

Key Points:
- We devised a numerical model for a probabilistic approach of the architecture of reef sequences: number and size of terraces and barriers
- The architecture of reef sequences is mainly driven by geological forcings: uplift or subsidence, and slope of the foundations
- The commonly assumed bijective relationship between sea level highstands and terraces is not systematic

Supporting Information:
- Supporting Information S1

Correspondence to:
A.-M. Pastier,
anne.morwenn@gmail.com

Citation:
Pastier, A.-M., Husson, L., Pedoja, K., Bézos, A., Authemayou, C., Arias-Ruiz, C., & Cahyarini, S. Y. (2019).Genesis and architecture of sequences of Quaternary coral reef terraces: Insights from numerical models. *Geochemistry, Geophysics, Geosystems*, *20*, 4248–4272. https://doi.org/10.1029/2019GC008239

Received 29 JAN 2019
Accepted 11 JUN 2019
Accepted article online 17 JUL 2019
Published online 30 AUG 2019

Abstract The variety of coral reefs morphologies highlights their sensitivities to several forcings; fossil reefs stack in sequences that are accordingly diverse. In order to understand their genesis and architectures, we devised a numerical approach, accounting for Quaternary sea level oscillations, vertical land motion, initial slope, wave erosion, and reef growth. We first test our model on the subsiding sequence of Hawaii and on the uplifting sequence of Wangi-Wangi (Sulawesi) that bears active barriers. We then construct a parametric study that we analyze based on a comprehensive yet compact description of sequences as *barcodes*, that depict the vertical distribution of a few geometrical characteristics (number, width, and height of the terraces and barriers). We find that geological factors suffice to explain the variety of architectures of reefal sequences at first order, regardless of additional ecosystemic processes. Vertical land motion and foundation slopes are the prime players, while reef growth rates only play a minor role. Barriers may develop both in uplift and subsidence mode, and their preservation attests for the erosional power. Last, we reappraise the genesis of sequences and find that sequences do not fingerprint discrete events of sea level oscillations but a continuous process harrowed by stochastic events: Major sea level fluctuations can be overrepresented by several terraces or conversely absent; reoccupations may yield composite terraces representing multiple events. Overall, sequences shall not be regarded as stacks of reef bodies forming during sea level highstands, which implies that the commonly assumed bijective relationship between sea level highstands and terraces shall be abandoned.

1. Introduction

The variety of coral reef morphologies and external architectures of sequences of coral reef terraces have triggered a quest to unravel the mechanisms at play which likely begins with Darwin (1842), Dana (1885), Agassiz (1903), or Daly (1915). Albeit these early studies focused on modern reefs, the question of their longer-term, Quaternary evolution was already germinated, in an attempt to unravel the competing effects of sea level change and vertical land motion. Scores of naturalist investigations followed the cruises of *HMS Beagle* (Darwin, 1831–1836) and *Vincennes* and *Peacock* (Daly, 1838–1842) and patiently documented some of the most remote reef systems, until today (e.g., Pedoja et al., 2018; Figure 1). Radiometric datings and descriptions of the morphologies at a high resolution complete modern analysis (see compilations of Hibbert et al., 2016; Medina-Elizalde, 2013). Yet, the overwhelming majority of these studies document localized sequences of fossil reefs, and attempts to unravel the controlling mechanisms mostly rely on discrete observations (e.g., Kennedy & Woodroffe, 2002; Montaggioni, 2005).

Herein, we attempt to overcome observational limitations with support from numerical simulations. As emphasized in several reviews (Braithwaite, 2016; Camoin & Webster, 2015; Montaggioni & Braithwaite, 2009; Woodroffe & Webster, 2014), numerical models are promising tools to alleviate this drawback. A number of studies now couple field observations to numerical models that are calibrated to reproduce observations (e.g., Barrett & Webster, 2012; Montaggioni et al., 2015). One step beyond is done to derive general behavior laws by taking advantage of the lessons learned from observations and mature modeling

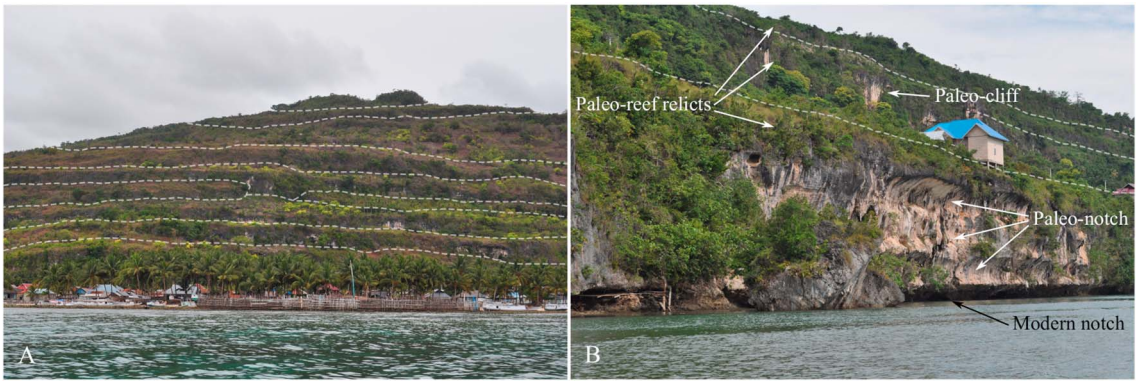

Figure 1. (a) Sequences of emerged reef terraces, Sampolawa Bay, SE Sulawesi (Fortuin et al., 1990; Pedoja et al., 2018). White dashed lines delineate uplifted terraces. (b) Close-up showing nested narrow terraces and fossil notches. The active notch is carving a retrograding cliff in earlier reefal units, which progressively erases earlier sea level markers. The erratic block in the forefront witnesses this retrogradation, while the preservation of fossil notches attests for moderate marine erosion.

techniques (e.g., Bard, Jouannic, et al., 1996; Toomey et al., 2013; Turcotte & Bernthal, 1984). In an earlier study (Husson et al., 2018), we endeavored to extract general rules based on a probabilistic approach, in order to quantify the worldwide productivity of carbonate reefs. We explored a full range of parameterizations instead of a unique model prediction based on a narrow parameterization. Similarly in the following, in an attempt to unravel the mechanisms that prevail to the first order, we evaluate a whole set of numerically reconstructed sequences of coral reef terraces in order to bypass intrinsic or ecosystemic effects that undoubtedly constrain the development of given sequences but prevent to generalize behavior laws. We thus mostly focus on extrinsic, geological forcings.

First, we devised a numerical model (as in Husson et al., 2018; Sarr et al., 2019) that accounts for Quaternary sea level oscillations, vertical land motion, initial slope of the foundations, coral reef growth rate, and marine erosion. Second, we test the robustness of this model by applying it to contrasting settings: The canonical subsiding sequence of Hawaii serves as a benchmark, while the original uplifting sequence of Wangi-Wangi (SE Sulawesi) is considered as a demanding test. Indeed, Wangi-Wangi displays barrier reefs in an uplifting environment. Because it is at odds with general concepts of reef development, as proposed by Darwin (1842), we consider it as a severe test to validate our modeling protocol. Third, we expand our approach toward a parametric study, in order to analyze the range of geometries and external architectures that can be achieved within a representative parametric space. We extract a few metrics, or geometric properties, to quantitatively describe reefal sequences. Then, we ultimately attempt to *barcode* them, in the sense that we aim for a general description of sequences by noting the vertical distribution of these properties. This could ideally permit to invert observations to retrieve the mechanisms at play.

2. Modeling Coral Reefs Sequences

Sequences of coral reef terraces shall not be regarded as linear stacks of paleoreefs, owing to the fact that coral reef terraces themselves shall not be considered as single paleoreefs (e.g., Pedoja et al., 2018). The joint effects of Quaternary sea level oscillations and marine erosion lead to reoccupations of fossil reefs, and these reoccupations commonly form composite terraces made up of multiple paleoreefs constructed during different Marine Isotopic Stages (MIS) or substages. We refer to these paleoreefs as reefal units. We define coral reef terraces by their morphological signatures, which include flat expanses separated by cliff steep slopes. They are limited landward by a break in slope, represented either by the foot cliff of the overhanging terrace or by the transition between the initial slope of the substrate and the morphological flat of the terrrace, and oceanward by their foot cliff or the transition between their steep slope and the initial slope of the foundations. Last, reefal sequences are defined as the aggregation of such terraces, whose morphologies and architectures respond to Quaternary glacial/interglacial cycles and marine erosion.

Numerical models started with the study of Chappell (1980), and a variety of more sophisticated models followed (e.g., Koelling et al., 2009; Toomey et al., 2013; Turcotte & Bernthal, 1984; Webster et al., 2007), often based on the formalism of Bosscher and Schlager (1992). These models are tentatively developed on physical grounds, where coral growth parameters depend on the insulation saturation in the water column.

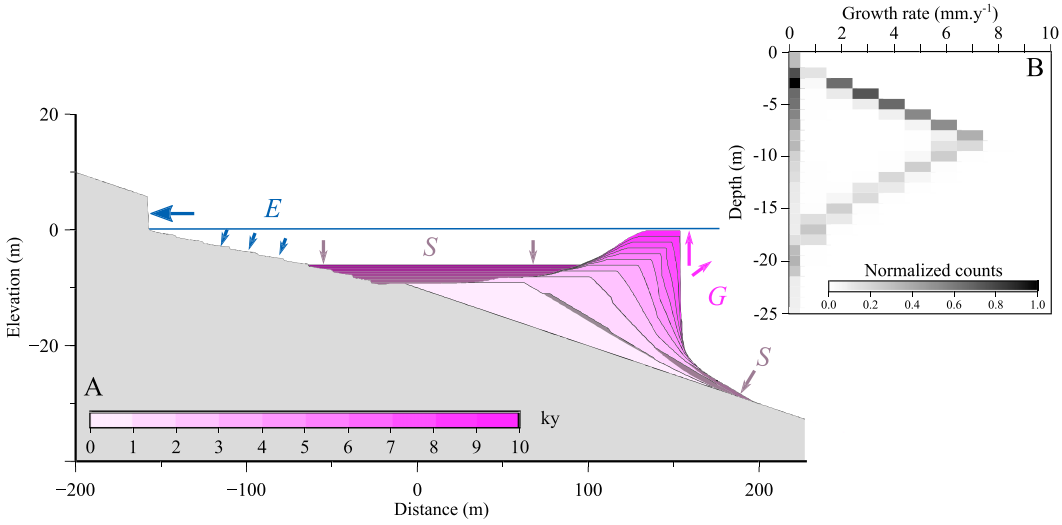

Figure 2. (a) Model output after a 10-kyr short simulation. Gray domain is the basement (initially having a linear surface), blue line is sea level, pink units are reef bodies, color-coded by age every 1 kyr. Shaded units are sedimentary layers. G, E, S, and U denote reef growth rate, erosion rate, sedimentation rate, and rate of vertical land motion, respectively. Parameters are as follows: stationary absolute sea level, $G^* = 10$ mm/year, $U = -1$ mm/year, $E^* = 3 \cdot 10^{-2}$ m^3/year, $\alpha = 10\%$. (b) Distribution of effective vertical reef aggradation rate for several simulations over 1.5 Myr. U ranges from −2 to 2 mm/year, $G^* = 10$ mm/year, $\alpha = 6\%, E^* = 20$ mm/year.

In this study, we instead propose a kinematic model based on reef morphology (as in ; Husson et al., 2018), defined by "effective" (or macroscopic) laws for reef growth G, marine erosion E, and clastic sedimentation S, as derived from the geological record (Figure 2a). A series of modules in the Fortran code sequentially treats reef growth, erosion, and sedimentation at each time and space steps (herein 1 kyr and 1 m, respectively). They depend on relative sea level as dictated by the joint effects of sea level oscillations and vertical land motion, as well as the morphology of the foundation.

2.1. Reef Growth

Most earlier reef growth models are based on the work from Bosscher and Schlager (1992) on the growth of a single species responding to light attenuation in the water column. But of course, many species adapt differently to light attenuation than *Montipora* sp. (as in Bosscher & Schlager, 1992). Moreover, individual coral colonies grow at rates higher than reef rates (e.g., Chappell, 1980; Dullo, 2005), whose growth potential is hampered by factors inherent to the structure of the reef (one could think of a *phase velocity* for individual colonies and a *group velocity* for the bulk reef). This variability prompted us to opt for an empirical description of an *effective* reef growth rate.

The reef growth module thus computes a growth rate, defined by a fraction of the potential reef growth rate G^* (the rate at which the reef would grow under optimal conditions). At any location along the 2-D profile, reef growth is defined as a slope normal vector. The magnitude of the growth vector is defined by the growth potential to which two penalties apply and curtail reef growth to local rates.

First, a vertical penalty factor γ applies, in order to account for the absorption of light in the water column, and modulates reef growth. The depth dependence is empirically defined by a sine function that declines to 0 at depth z_{max}, such that

$$\gamma = \frac{1}{2}\left(1 + \cos\frac{\pi h(s)}{z_{max}}\right), \quad (1)$$

where $h(s)$ is the local depth along the profile. In addition, at shallower depths than z_{min} (the shallowest segment where waves are active), the penalty coefficient linearly decreases upward to 0 at the surface. Second, a horizontal penalty factor ζ is computed in order to account for increasing turbidity and decreasing wave oxygenation shoreward, which hamper reef growth. The horizontal distance to the open water ($x_{ow} - x$, where x_{ow} is defined by a minimal water depth z_{ow}) is plugged in the penalty factor, such that

$$\zeta = \frac{1}{2}\left(1 + \tanh\frac{x_{ow} - x}{\delta}\right), \tag{2}$$

where δ sets the horizontal tension. Landward, this penalty ensures that the production is focused at the reef crest; oceanward, its effect is most often superseded by the vertical penalty function in the one hand and by the fact that the model systematically trims unrealistic overhanging reefs. Only when the bathymetry at greater depths than z_{ow} declines very gently does tanh play a role oceanward, which ensures a gradual transition toward the open water and greater depths. Last, the reef growth vector is of course always truncated in the vertical direction by the relative height of the water column. At any location, the effective reef growth rate thus writes

$$G = \gamma \times \zeta \times G^*. \tag{3}$$

The range of growth rates and the general parametrization is based on observations of coral colonies. In the following, G^* is assumed constant throughout glacial cycles. This assumption is supported by the observations of Crabbe et al. (2006) on individual colonies throughout the Quaternary and further supported by the analysis of coral communities by Pandolfi and Jackson (2006). z_{max} is set according to field observations (Dullo, 2005; Bosscher & Schlager, 1992; Montaggioni, 2005). In practice in our simulations, because of the penalties γ and ζ applied to G^*, the effective reef growth rate is systematically lower than the maximum potential growth rate G^*. An example of the distribution of growth rates for a given range of simulations is shown in Figure 2b, where G never exceeds ~7 mm/year, while G^* is set to 10 mm/year. This difference explains the apparently high values of G^* used in this study, allowing G to match reef growth rates, as in Bosscher and Schlager (1992), albeit based on a kinematic approach.

2.2. Erosion

The erosion module derives from the model of Anderson et al. (1999). We define the erosional potential E^*, to account for tidal and wave energy but also on chemical and biological agents. This value is poorly known, and we simply express it as an effective eroded volume per unit time (and per unit length of coast, for the model is two-dimensional). The erosional potential is dissipated from the open ocean toward the shore, making the erosional residual power E_r gradually decrease shoreward. At each location along the profile, a fraction of E_r erodes the foundation. That fraction is defined as a function of true local depth $h(s)$ along the curvilinear profile s and a coefficient of bedrock erodibility K, such that

$$\frac{\partial E_r}{\partial s} = K \times E_r \times \exp(-\frac{h(s)}{z_0}), \tag{4}$$

where z_0 is the typical depth of wave action. The remainder is computed at each step along the profile and resets E_r until the shore is reached, where the residual power $E^* - \int_s \frac{\partial E_r}{\partial s}\,ds$ serves to carve a 1-m-high notch. All the overhanging material collapses to form a cliff. Subaerial erosion over higher landscapes (mostly chemical erosion and karstification for intertropical reef carbonates) is considered negligible over the time scales considered.

2.3. Sedimentation

The sedimentation module computes and redistributes the eroded material, including the bedrock, notch, and fallen cliff. It operates seaward from the shore, and deposits start at depths greater than critical depth z_0. Lagoons, if any, are preferentially filled up to depth z_0 with horizontal layers. The remainder is transported further seaward, on the slope of the fore reef, and is disposed at an arbitrary rest angle θ (or critical sediment slope).

2.4. Absolute Sea Level and Initial Topography

Glacio-eustasy, initial slope, and vertical land motion complete the setup. Absolute sea level is given at each time step from a composite curve (Figure 3) designed on the basis of the reconstructions of Waelbroeck et al. (2002) for the most recent 430 kyr (Figure 3b) and Bintanja et al. (2005) from 430 to 3,000 ka. We opted for this concatenation to take the respective advantages of the two sets. On the one hand, Waelbroeck et al. (2002) provide the result of a compilation of several proxies from different parts of the global ocean (and as such thought of as most representative), and their sea level curve includes high frequencies of sea level variations. On the other hand, the curve of Bintanja et al. (2005) covers a longer time span that ensures that the initial conditions (for the initial morphology of the basement in particular) are obliterated at present

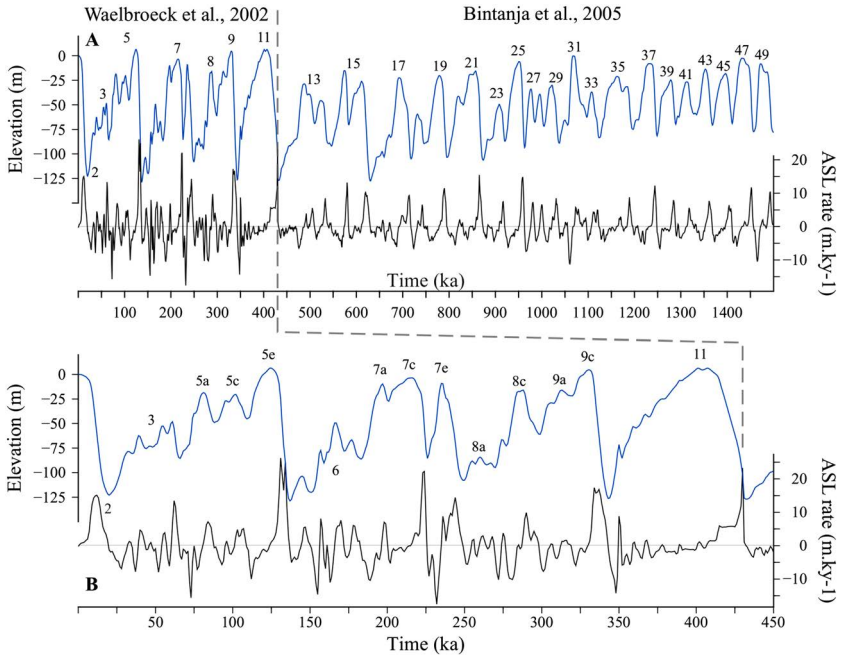

Figure 3. Absolute sea level (ASL) reconstruction used in this study. (a) Blue curve shows composite eustatic reconstruction (concatenated from Waelbroeck et al., 2002 [0–430 ka] and Bintanja et al., 2005 [431–1,500 ka]). Numbers identify isotopic stages or substages. Black line shows the rate of ASL variations for the composite reconstruction. (b) Detailed view of ASL reconstruction since 450 ka (blue line) and rate of ASL variations (black line). Dashed line bounds the two reconstructions.

day, but at a poorer resolution. Of course, any alternative curve from the disconcerting set of available curves (see discussion by Caputo, 2007) could be implemented.

Vertical land motion U, for either subsiding or uplifting shorelines, is ultimately imposed. They typically range between −2 and 2 mm/year worldwide Pedoja et al. (2014). In our models, we use constant rates throughout, but more complex histories can naturally be implemented instead.

Table 1
Parameters and Symbols

Symbol	Definition	Value and unit
G^*	Potential reef growth rate	5 to 20 mm/year [10 mm/year]
z_{ow}	Minimal depth for the open water	2 m
z_{max}	Maximum reef growth depth	10 to 50 m [20 m]
z_{min}	Optimal reef growth depth	1 m
γ	Vertical reef growth coefficient	—
ζ	Horizontal reef growth coefficient	—
δ	tanh tension for reef growth decay from the open ocean	20
E^*	Erosional potential	10^{-2} to $4 \cdot 10^{-2}$ m^3/year [2.10^{-2}]
z_0	Reference depth for wave action	3 m
K	Coefficient of erodibility	0.1 (bedrock) / 1 (notch)
θ	Critical sediment slope	10°
α	Initial slope	2% to 14% [6%]
U	Uplift rate	−2 to 2 mm/year

Note. Bracketed values denote the reference case

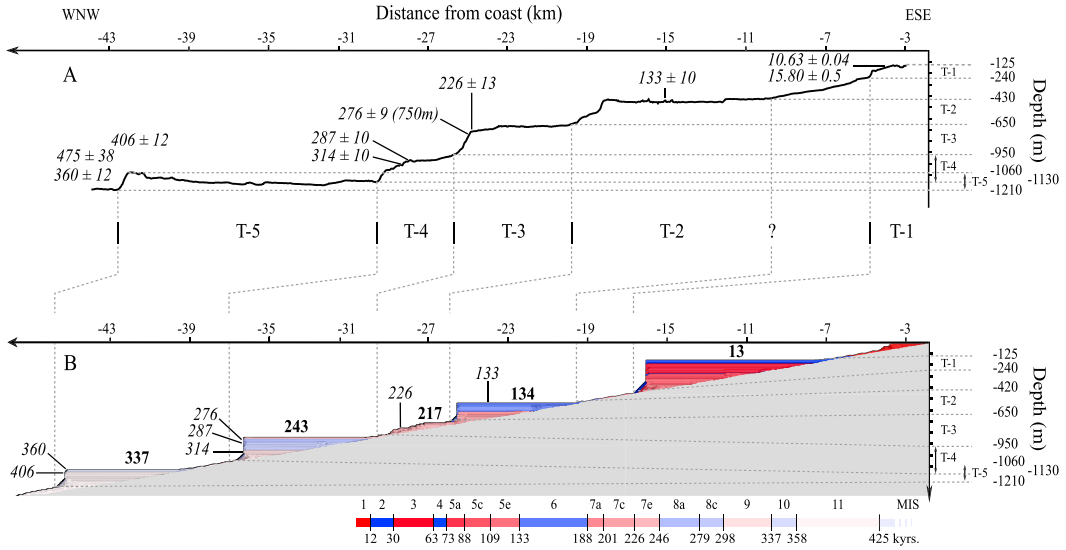

Figure 4. (a) Bathymetry of the NW Hawaii sequence (from MBARI Mapping Team, 2000). Dated samples (ages in ka are italicized) are either found along the profile or projected laterally (from Ludwig et al., 1991; Webster et al., 2007). (b) Modeled architecture of the reef sequence for the best fitting simulation, with equivalent locations for dated samples (italicized) and last age of construction for each terrace prior to abandonment (in bold). Color scale shows glacial (blue) and interglacial (red) isotopic stages; color saturation denotes age and increases with younger ages. Parameters: composite sea level curve concatenated from Waelbroeck et al. (2002) and Bintanja et al., 2005 (2005; see section 2.4), $U = -3$ mm/year, $\alpha = 3\%$, $G^* = 7$ mm/year, $z_{max} = 50$ m, $E^* = 5 \cdot 10^{-2}$ m^3/year.

Last, the initial morphology is defined by a uniform slope α. In the following, we vary the basement slope between 2% and 14%, which is typical of most coasts, but again, alternative situations could more appropriately apply to real cases provided it can be documented. Table 1 summarizes the overall parametrization of the model.

3. Case Studies

In order to test our model, we simulated the evolution of two reef sequences, chosen for their differences in terms of coral growth and vertical land motion. The first one is the well-documented subsiding sequence of Hawaii, which has already been modeled by Webster et al. (2007) and Toomey et al. (2013) and therefore serves as a benchmark for our model. In addition, fast subsidence makes it an interesting case for our modeling approach. The second is the original uplifting sequence of Wangi-Wangi, SE Sulawesi. Its atypical uplifting active barrier reef, only briefly described in earlier literature, serves as a rigorous and severe challenge to validate our modeling approach. The model is tested forward over 1.5 Myr, using uniform slopes, steady vertical land motion rates, and the composite sea level curve derived from Waelbroeck et al. (2002) and Bintanja et al. (2005) and is adjusted by trial and error.

3.1. Hawaii

Hawaii subsides as a response to the volcano load on the oceanic crust (e.g., Huppert et al., 2015; Watts & Ten Brink, 1989). The shores of the archipelago host a range of coral reef morphologies, from narrow fringing reefs around the youngest island of Hawaii to atolls or table reefs for the eldest, now drowned, volcanoes (e.g., Sand island and Green island). On the northwestern shore of Hawaii island, the reefal sequence shows few but very wide drowned terraces (five terraces, 4 to 13 km wide, as deep as −1,060 m) that were dated (U/Th on sampled or dredged corals) and largely described (compiled in Figure 4 ; Ludwig et al., 1991; Moore & Fornari, 1984; Moore et al., 1990; Webster et al., 2004). The 125-m deep *T-1* main terrace is dated at ~15 ka from in situ samples (with the youngest age at 10.6 ± 0.04 ka ; Webster et al., 2004). This last episode of reef construction marks the drowning of the reef unit. The timing of the associated *give-up* response of the reef marks the time at which reef growth ceases when the rising relative sea level precludes further reef growth, as described by Neumann and Macintyre (1985). The 430-m deep *T-2* is dated with a single sample at 133 ± 10 ka (provided the terrace is laterally continuous, for the sample was taken further south). *T-3* lies at −650 m; three samples associated with its upper surface yield ages at 225 ± 12 and 226 ± 13 ka.

Another sample from its fore reef is dated at 276 ± 9 ka. Samples from the 950-m deep *T-4* terrace are dated at 287 ± 10 ka (sampled at 960 m) and 314 ± 10 ka (at 980 m). *T-5* lies at −1,130 m and is dated from a dredged sample on its distal part at 406 ± 12 ka, and from in situ samples dated at 475 ± 38 ka (at 1,110 m deep) and 360 ± 12 ka (at 1130m). This terrace is tilted at 0.5% toward the island.

The sequence has already been modeled by Webster et al. (2007) and Toomey et al. (2013), respectively yielding mean subsiding rates of −2.5 and −2.6 mm/year. Webster et al. (2007) focused only on T-1 and T-2 and used a different reconstruction for sea level variations (Lea et al., 2002). They successfully reproduced terrace depths, T-2 width as well as their drowning ages. They also used their model to predict reef stratigraphy. Toomey et al. (2013) focused on the morphology of the four shallowest terraces. Their model yields an additional terrace and too narrow terraces.

Our best fit simulation (Figure 4b and supporting information Movie S1) shows good agreement with the data. The simulation was run forward from 430 ka, as the fast subsidence rate prevents reoccupation of former possible reefs. With a slightly faster subsidence rate of −3.0 mm/year, the morphology of the sequence is satisfactorily predicted, with five wide terraces, the older terraces lying deeper. The model predicts a drowning age for T-1, here the most recent terrace, at 13 ka, in agreement with Webster et al. (2007) although vertical rates slightly differ. Pursuing backward in time, the model reveals that T-1 was constructed during MIS 5 to MIS 3 sea level variations, almost continuously. The fast transgression prior to MIS 5 led to the sudden and quick drowning of T-2, which is predicted by the simulation at 134 ka, in agreement with available datings. According to our simulation, terrace T-2 was finally constructed during MIS 6, when the sea level reoccupied the antecedent foundation built during the MIS 7a and 7c sea level variations. In our simulation, terrace T-3 is the only monogenic terrace and was achieved at 217 ka. The reef *gave up* during the fast MIS 7c transgression (Figure 3b) in agreement with the datings. The latest episode of construction of T-4 predicted by the simulation occurs at 243 ka, being abandoned thereafter, due to the fast transgression of MIS 7e, consistently with the dated samples from the fore reef. The simulation further predicts a drowning age at 337 ka for T-5, which is once again in agreement with the samples in the fore reef.

While our simulation of the Hawaiian sequence satisfyingly reproduces the five terraces, some differences in elevations and width persist. Predicted depths for T-5 and T-1 are in good agreement with the data, whereas T-2 and T-3 are deeper than observed (by 80 and 40 m, respectively) and T-4 is shallower by 100 m. These differences could be due to the uncertainties in eustatic variations or to temporal and/or spatial variability in subsidence rate along the profile. The fact that T-5 is tilted supports this hypothesis, as well as the current GPS data showing both current subsidence and uplift on different sites of the island. The apparently large mismatch between observed and predicted widths (−7 km for T-5, +6 km for T-4, and −4 km for T-3) simply highlights the fact that slight variations in the overall shallow Hawaiian slopes (∼ 2.5%) very efficiently modulate terrace widths. Last, our simulation does not fit one dated sample (276 ka). While the current depths of the other samples support a −3.0 mm/year subsiding rate, regarding their ages and the eustatic reconstructions, this outlier, sampled at −750 m, is located between 843 and 920 m deep in our simulation. The difference between theoretical and actual depths can be explained by the strong uncertainty associated with the elevation of sea level during MIS 8c or by a nonlinear subsidence rate, or by a combination of both.

In this sequence, subsidence and growth rates allow the reef to *keep up* during minor transgressions (e.g., 5a and 5c). Similarly, relatively slow regressions (e.g., 7c and 5c; see Figure 3b) do not lead to the emergence and abandonment of the reef but let the reef keep pace with the fast subsidence. Only relatively fast regressions (e.g., 5a, 7a, and end of MIS 11 regression) lead to short-lived and intermittent periods of emersion of the reef, as proposed by Webster et al. (2007). These episodes lead to a period of negligible construction as falling relative sea level sweeps the steep foreslope of the anterior reefal construction. This configuration offers narrow and steep foundations that are not prone to reef development. Subsequent transgressions entirely reoccupy the former reef after this stage and expansion resumes. Successive reoccupations lead to the construction of kilometer scale terraces. Reefs are eventually drowned during the fastest transgressions (e.g., MIS 11, 9c, and 5e) when fast subsidence and fast sea level rise jointly exceed the reef potential growth rate, leaving glacial stage reef flats cap the terrace prior to abandonment. This is almost systematically reflected in the terraces T-4, T-2, and T-1 (see more details in the parametric study, section 4, and section 5.2).

Hawaii sequence shows few terraces and a high absolute vertical rate. Subsidence seems to be responsible for the limited amount of permanently abandoned reefs, for emerged reefs after regressive episodes are always reoccupied and keep-up prevails during minor transgressions. It is noteworthy that these results can

be readily compared to fast uplifting counterparts, such as the Huon Peninsula (Chappell, 1974), that shows multiple narrow terraces. In the fast subsiding Hawaiian sequence, these reoccupations and keep-ups also explain the impressive width of the terraces. The favorable geometry of the foundations of each reoccupied reef promotes the development of wide platforms. The very gentle initial slope (3%) is also very influent on this last criteria. The terraces show a great variability in width (by a factor of 3). As subsidence always provides accommodation space, the width of a terrace could be directly correlated to the duration of occupation and construction of the reef. Last, this subsiding sequence does not exhibit any barrier reef, which could be due to the very fast subsidence and/or moderate reef growth rate (see section 4).

3.2. Wangi-Wangi

The Tukang Besi archipelago (also known as Wakatobi), in SE Sulawesi, forms a NNW trending array of coalescent islands, more than 100 km long and less than 20 km wide at its maximum, mentioned in the literature by Kuenen (1933), Pedoja et al. (2018), Satyana and Purwaningsih (2011), Tomascik et al. (1997), and Verbeek (1908). This small continental block collided with Buton island at about 3 Ma (Fortuin et al., 1990), which subsequently led to the widespread emersion of Quaternary reef sequences on both sides of the collision. In Tukang Besi, the ubiquitous veneer of Quaternary coral reef terraces that almost entirely covers the islands obviously records this episode of recent uplift. The northernmost island of Wangi-Wangi (cf. Figure 5b) displays several well-defined terraces of variable widths (up to several hundred meters wide). It is gently tilted southwestward, as already noticed a century ago by Verbeek (1908). The island peaks at ~250 m, and overall slopes vary between 2% and 5.5%.

Most specific to Wangi-Wangi is its remarkable barrier reef, which stretches along the northeastern part of its shoreline. This poorly studied feature (Pedoja et al., 2018; Tomascik et al., 1997) attracted our attention, not only because it challenges the general wisdom that assigns barrier reefs to subsiding domains but also because we purport that it should be characteristic of a very specific regime and as such should be a demanding test to benchmark our model. To our knowledge, fossil emerged barriers are seldom described in the literature. Such examples can be found at the Huon Peninsula but in more modest proportions (up to a maximum of 10 m above the lagoon; Chappell, 1974), at Lifou island and Ouvea atoll (Andréfouët et al., 2009), or Tuvuca Island (Nunn, 1999). The reef in addition shows a strong lateral variability within a few kilometers of coastal stretch, from a single fringing reef along the western coast, diverting in a barrier reef to the north and even to twin barriers along the eastern coast (Figure 5b). The barrier reefs of the northwestern shore are punctuated by laterally periodic pools (in situ measurements indicate depths of 10 to 40 m, data from sonar measurements acquired by the authors in 2016). Interestingly, the onshore fossil sequence reveals comparable features, as paleolagoons and paleobarrier reefs, up to 40 m high, are noticeable in the topography (see Shuttle Radar Topography Mission (SRTM) Digital Elevation Model (DEM); Figure 5b).

The studied reef sequence of Wangi-Wangi is located on the northern shore (Figure 5b). It shows a single barrier with blooming corals forming a narrow lagoon bordered by the 300-m wide modern platform (Figure 5d). A smaller fringing coral reef is confined to the platform's foreslope. This shallow platform is covered by seagrass in its submerged portion gradually converting into a sandy unit ultimately bounded by a fossil notch at the cliff foot of the first terrace T-1 at an elevation of 1.5 m above sea level (Pedoja et al., 2018). On this platform stands an emerged sea stack (Figure 5c), either inherited from the erosion of terrace T-1 or a former apron. Two fossil notches are visible in the cliff of T-1; at 4 ± 1 and 7 ± 1 m above sea level T-1 is 800 m wide and its roughness differs from north to south. The altitude of T-1 varies from 11 m in its most distal part to 17 m at the cliff foot of T-2. Two samples were dated, GSL-2013-50 and GSL-2013-54, respectively, at 133 ± 4 and 131 ± 4 ka (Pedoja et al., 2018), corresponding to the last episode of transgression of MIS 5e. The two higher terraces exhibit small scarps (about 10 m high) and uniform widths of about 500 m. They are overhung by what we interpret as a fossil barrier reef, with a much higher scarp (~40 m). Based on a morphostratigraphic interpretation of these datings, Pedoja et al. (2018) proposed an uplift rate of 0.13 ± 0.11 mm/year.

The fast sea level variations at the age of the dated samples yields an important uncertainty in Relative Sea Level (RSL) that precludes better bracketing of uplift rates than a range of 0.05 to 1.0 mm/year. The morphology of the reefal sequence, including the presence of the modern barrier, is then used to refine the estimation of the vertical rate. Our best fit simulation of the sequence results in a preferential rate of 0.10 mm/year (Figure 5b). Indeed, at higher rates, the predicted morphology of the sequence has too many, too narrow, and too high terraces. In addition, although the width of the predicted modern barrier is exaggerated, its

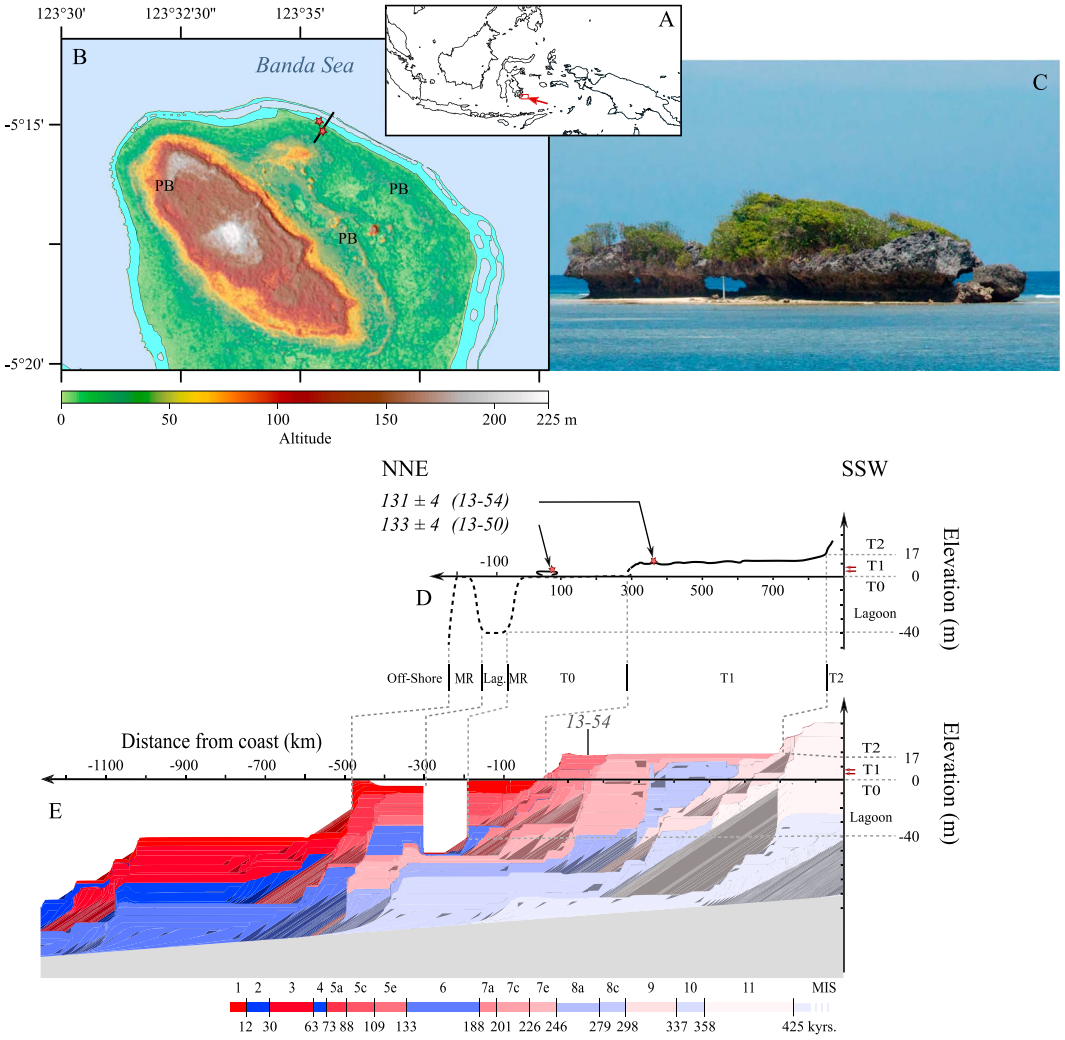

Figure 5. Wangi-Wangi island. (a) Location of the Tukang Besi archipelago, Indonesia. (b) Topographic map of northern Wangi-Wangi (SRTM30): light blue area shows modern reefs and platforms, PB = paleobarriers, black line shows location of the detailed topographic profile, and red stars location of dated coral samples. (c) Emerged sea stack, relict of the fossil sequence, location of the northernmost sample, GSL-2013-50. (d) Synthetic topographic profile from differential Global Positioning System and sonar records, stars locate the dated samples. (e) Best fit simulation from the terrace model ($U = 0.1$ mm/year, $\alpha = 2\%$, $G^* = 15$ mm/year, $E^* = 30$ mm^3/year). Color scale as in Figure 4b.

presence is a critical criteria to determine the best field of parameters, not only for vertical rate, but also for potential reef growth and wave erosion. A single-barrier reef requires an uplift rate between 0.08 and 0.14 mm/year, potential reef growth rate between 14 and 16 mm/year, and maximum erosional potential of $3 \cdot 10^{-2}$ m^3/year. This result is in good agreement with the morphostratigraphic interpretation of (Pedoja et al., 2018). We are also able to reproduce the twin barriers that only appear for a very narrow parametric window ($0.12 \leq U \leq 0.13$ mm/year, $G^* = 14$ mm/year, $E^* = 20$ mm/year), which attests for a gentle eastward increase of uplift rates (Figure 5b).

The simulation obtained with an uplift rate of 0.1 mm/year reproduces well the elevation and width of T-1. This terrace marks the highstand of MIS 5e but would be the result of several reoccupied MIS stages (5e, 7a, 7c, 7e, 8e, and 9; cf. Figure 5e). For such a vertical land motion rate, these highstands coincide between 15 and 20 m high. Each of these highstands reworked the former terrace and built a new reef in front of the preexisting one, sometimes even over it, as during MIS 7e in our simulation. This episodic construction could explain the roughness of T-1. Marine erosion leveled down the minor differences of elevation and facilitated the successive episodes reoccupations. At last, the reef possibly built a veneer during MIS 5e on the preexisting favorable foundations, thus hiding the composite nature of this terrace. Terrace T-2 could

have been built on the same process, at least from MIS 9a, 11, 13, and 15. Our modeled sequence suggests that T-1 is a composite terrace and that contiguous terraces may not always arise from contiguous isotopic stages. This pattern is also found on the older part of the profile (not presented here), which reproduces paleobarriers formed during several MIS.

The width of the modern platform *T-0* is well reproduced in our simulation. In agreement with Pedoja et al. (2018), it would be mainly formed by reef accretion during the Holocene transgression on the favorable foundation of the superimposed paleoreefs from MIS 6, 5c, and 5a. Wave erosion would be a minor component, eroding the cliff foot of T-1. Finally, according to our simulation, the modern barrier reef would also result from a multistage construction process. The best fit simulation shows that it nucleates during the transgression of MIS 7e. As the initial barrier resisted to erosion during the following regression, it was then self-maintained by the advantageous foundation of the available accommodation space over the MIS 6, 5e, 5c, 5a, and Holocene transgressions (see supporting information Movie S2). The 7e, 7c, and 5e transgressions were too fast for the barrier reef to keep up and it got drowned. Since the 5c transgression, the barrier reef is well developed, prevents the growth of the inward platform, and thus shields the lagoon from further reef growth. This implies that the reef barrier resisted to aerial erosion notably during MIS 2 and 3; this hypothesis is indirectly supported by the fact that similar paleobarriers further inland are also very well preserved in the topography (Figure 5b).

The location of the sample GSL-2013-50 is not satisfactorily reproduced in the simulation. Moreover, the latter predicts that T-0 results from reef accretion much more than from wave erosion. We thus suggest that the emerged sea stack where sample GSL-2013-50 comes from does not correspond to the distal edge of a uniformly wide former terrace but to the distal edge of an apron, eroded on both sides due to wave refraction and may then not be representative of a former topography for the area. Such aprons are indeed visible in the modern reef on the northeastern shore of the island. The simulation shows an additional drowned terrace at −40 m below sea level. This is due to the initially uniformly sloping topography. Indeed, in situ sonar measurements indicate a steep slope off the barrier and an increasing bathymetry down to depths below −120 m.

The sequence of Wangi-Wangi shows less terraces than the sequence of Hawaii (respectively two and five terraces since 430 ka). This is due to the slow uplift rate at Wangi-Wangi, which promotes reoccupations during successive glacial/interglacial cycles (Bard, Jouannic, et al., 1996). On the opposite, although the initial slopes were possibly comparable, the more frequent reoccupations produce narrower terraces (several hundred meters in Wangi-Wangi, as opposed to several thousand meters in Hawaii). This indicates that the uplift promotes the saturation of the accommodation space by reef construction (see parametric study, section 4).

3.3. Insights From the Hawaiian and Wangian Case Studies

These two contrasted studies illustrate remarkably different behaviors. Overall, we note that the uplifting sequence of Wangi-Wangi shows less terraces than the subsiding sequence of Hawaii (respectively two and five since MIS 11). This is due to the slower absolute vertical rate at Wangi-Wangi. Terraces in Hawaii are much wider than in Wangi-Wangi, and we hypothesize that it is due to the subsiding (and not uplifting as in Wangi-Wangi) regime. Interestingly, as opposed to the general wisdom since Darwin (1842), the uplifting Wangi-Wangi island exhibits a modern barrier as well as few fossil barriers, while subsiding Hawaii exhibits no barrier whatsoever. These conflicting views indicate that both in subsidence and uplift, the barrier regime resides in narrow parametric fields and should not be regarded as a symptomatic feature of drowning islands. Finally, samples from Hawaii mainly indicate give-up times within glacial stages while at Wangi-Wangi, our simulation suggests that last episodes of construction prior to abandonment are associated with interglacial stages. This fundamental difference is also likely reflecting the contrasted regimes of vertical land motion.

The mismatch between observed and predicted terrace widths could reveal that close adjustments to the local slope expand the active domain by several kilometers, which we did not account for in both case studies. Similarly, small elevation offsets could reveal that uplift rates were not as steady as in our simulations or point to uncertainties of the chosen absolute sea level (ASL) curve. Of course, we could have tuned these boundary conditions to a finer degree, allowing for more complex initial morphologies and time and space variations of subsidence rates, until model predictions match observations to the desired degree. But in the absence of further constraints the exercise would not be much relevant and lies beyond our scope.

The analysis of Toomey et al. (2013) refined the earlier study of Turcotte and Bernthal (1984), and both showed that the morphology of the sequences of coral reef terraces bear some information on the parameters that lead to their edification. In the current study, the two contrasted case studies of Hawaii and Wangi-Wangi confirm that the detailed morphological architecture of reefal sequences is a parametric barcode, in the sense that it can be used to retrieve the conditions that prevailed during the edification of the sequences. Below, we therefore propose a systematic analysis of a few metrics that describe such barcodes and perform a parametric study to tentatively extract general behavior laws to a higher degree of precision than those earlier studies.

4. Parametric Study

In order to achieve a quantitative and comprehensive analysis of the architecture of reefal sequences, we performed 2,624 simulations, incrementally varying four parameters: uplift or subsidence rate U, potential reef growth rate G^*, initial slope α, and erosion potential E^*. Our analysis often refers to reference values for G^* (10 mm/year), α (6%), and E^* ($2 \cdot 10^{-2}$ m^3/year), all other parameters but vertical rate remaining fixed (Table 1). For each simulation, we extracted the number of terraces, the number of modern and fossil barrier reefs, the widths and heights of the terraces, and the variability of their widths and heights within a sequence and extract the MIS associated with the latest reefal unit of a given terrace or barrier prior to abandonment.

Prior to considering all results at once, Figure 6 shows three simulations for the reference parametrization. In the stationary scenario ($U = 0$ mm/year), two principal emerged terraces formed during several isotopic stages corresponding to the highest sea level stands (MIS 11, 9, and 5e). Wave erosion due to the last interglacial maximum (MIS 5e) leveled out earlier terraces and only moderately expanded the reef body seaward, as the accommodation space was already saturated by ancient reefal units. Contrarily, lower former platforms constructed during MIS 5c and 5a provided favorable foundations for the Holocene reef that abundantly expanded. More generally, each transgression saturates the accommodation space, but sedimentation due to wave erosion, as well as platforms constructed during low sea level stands, rejuvenate the accommodation space so that it provides at each time more favorable foundations during the following transgression. In the absence of uplift or subsidence (or for small absolute rates, of a few tenths of millimeters per year) the reef progrades on its own sediment and forms a unique reef body. At higher rates ($U = 1$ mm/year or $U = -1$ mm/year in Figures 6a and 6c), the sequence stretches and distinct terraces appear (comparable to Turcotte & Bernthal, 1984, and Bard, Jouannic, et al., 1996). At an equivalent absolute rate, subsidence generates fewer but wider terraces than uplift, because the keep-up regime prevails for much longer time spans during subsidence. Last, these contrasted examples suggest that more fossil barrier reefs are preserved during subsidence than during uplift.

The following analysis considers all the 2624 simulations, to more systematically explore the impact of uplift or subsidence rate U, potential reef growth rate G^*, initial slope α, and erosion potential E^* on the number of terraces formed during the entire simulation time (Figure 7a), their widths and width variability (Figure 7b), and the number of fossil barrier reefs (Figure 7c).

4.1. Number of Preserved Terraces

The prominent observation is that the number of terraces primarily depends on the vertical rate, regardless of initial slope α, potential growth rate G^*, and erosional potential E^* (Figure 7a, left, middle, and right panels). All modeled sequences show more terraces with increasing absolute rates, both in subsidence and uplift. This is due to the decreasing frequency of reoccupation of earlier reefal units as vertical rates increase: vertical land motion withdraw antecedent reefs from the range of sea level oscillations, therefore more efficiently preserving former markers of sea level variations. The amount of terraces does not increase infinitely, however, and reaches a maximum number that corresponds to the number of independent sea level oscillations. In the absence of vertical land motion, all units coalesce and form a single terrace, in spite of sea level oscillations.

To a second order, uplift more efficiently than subsidence promotes the development of sequences where more terraces are developed, twice as many terraces being found in uplift than in subsidence mode. On uplifting coasts, earlier reefs are gradually abandoned during emersion: Reefal units constructed during major interglacial stages (MIS 5e, 7c, and 9c) are withdrawn from the system during their emersion and are thus less likely to be reoccupied during following transgressions. Reefs constructed during minor interglacial (MIS 5a and 5c) or glacial stages (MIS 2, 4, and 6) and drowned during their subsequent transgression are

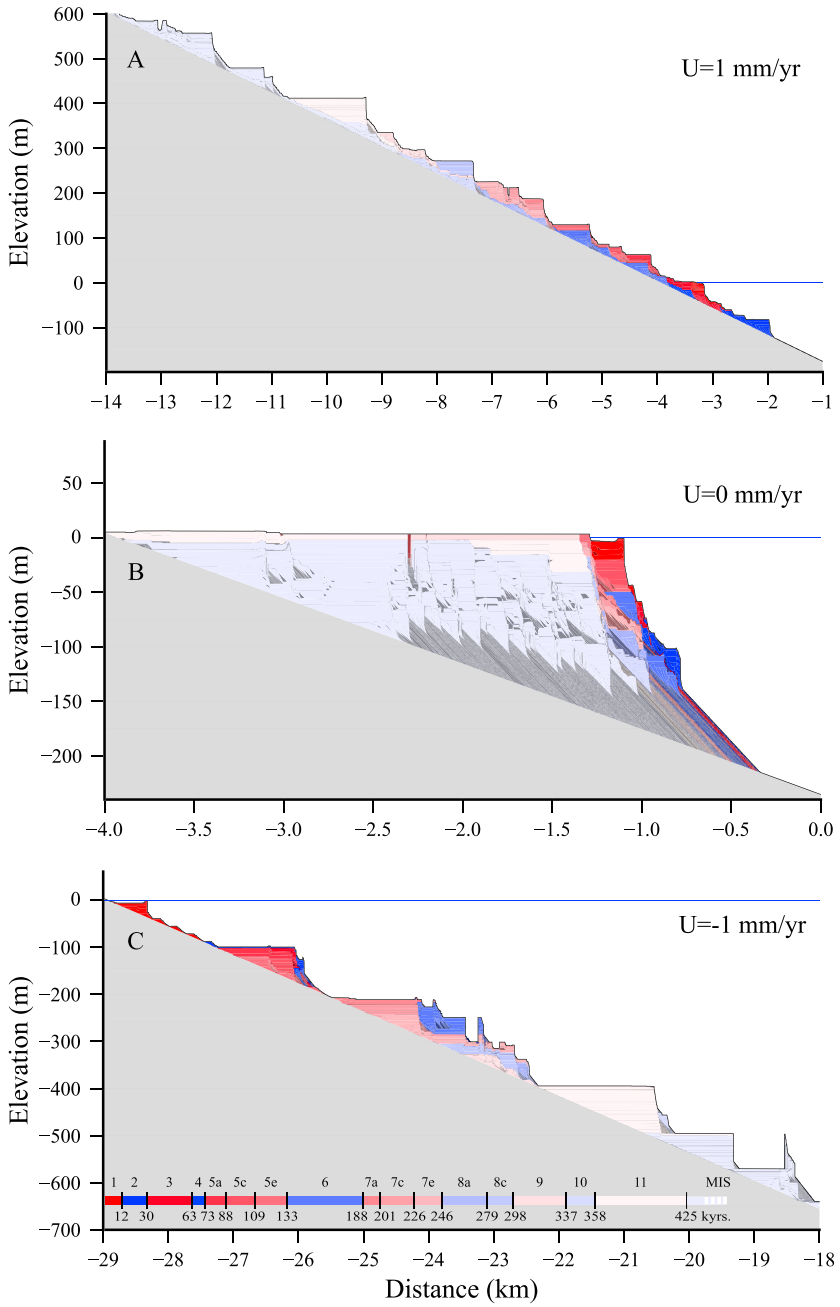

Figure 6. Simulations for three contrasted vertical rates: (a) fast uplift, 1 mm/year; (b) stationary, 0 mm/year; (c) fast subsidence, −1 mm/year (for reference values $G^* = 10$ mm/year, $\alpha = 6\%$, $E^* = 20$ mm/year; other parameters as in Table 1). Time evolution animations are provided online (supporting information).

most likely reoccupied for modest uplift rates, but the frequency of this process decreases with increasing uplift rates.

On subsiding coasts, reefs formed during interglacial stages emerge during glacial stages but are reoccupied by the subsequent transgression. Reefs are eventually abandoned by drowning. Increasing subsiding rate increases relative sea level rise, which exceeds the maximum effective reef growth rate more often. Give-up occurs more often, and in turn more terraces are preserved. For stable coastlines (or at low rates of uplift or subsidence), very few terraces (up to four) form, corresponding to the highest highstands (e.g., MIS 5e and MIS11), but overall the entire accommodation space is quickly occupied, which prevents efficient reef development (Husson et al., 2018). Low vertical land motion promotes the development of a unique, massive

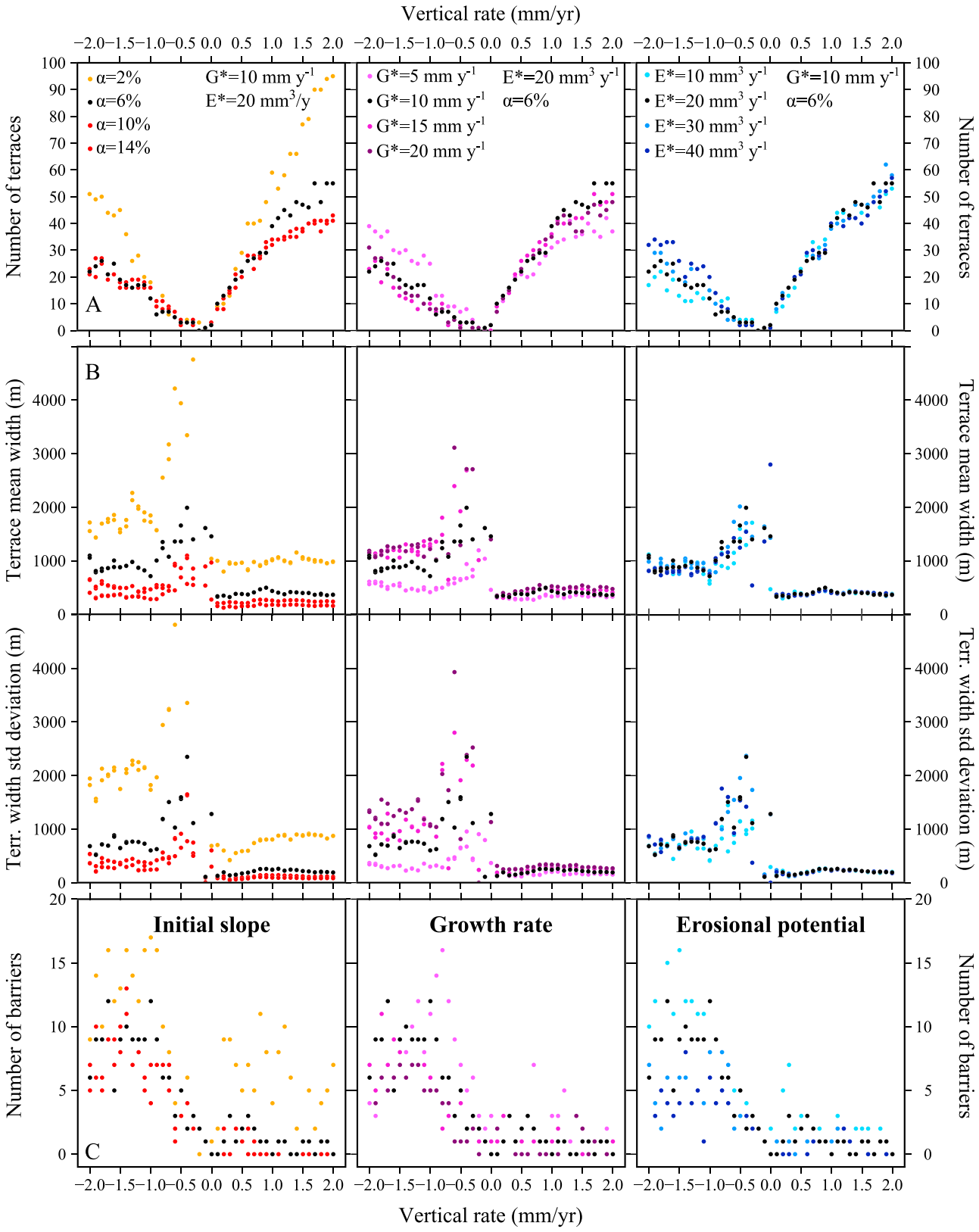

Figure 7. Systematics of modeled reefal sequences architectures, for variable sets of parameters with respect to reference values (black dots, $G^* = 10$ mm/year, $\alpha = 6\%$, $E^* = 20$ mm/year; other parameters as in Table 1), varying slope α (left column), potential reef growth G^* (middle column), and erosion potential E^* (right column). (a) Number of terraces in reefal sequences, (b) average width and standard deviation of the width of terraces, and (c) number of preserved modern and fossil barrier reefs.

terrace, and only the prograding sedimentation, along with reefs formed during lowstands, rejuvenates the foundation and allows for the reef to slowly continue prograding seaward.

The second most influent parameter is the initial slope (Figure 7a, left), which increases the number of preserved terraces by a factor of 2, approximately, for α ranging from 2% to 14%. Steepest slopes show the lowest amount of terraces for both uplifting and subsiding sequences, because they offer smaller accommodation space, quickly saturated by reef construction. Large accommodation spaces on low slopes are conversely less commonly saturated. Finally, steep slopes enhance erosion of coastal cliffs and therefore sedimentation of the eroded material on the slope of the forereef, which erases and masks previous minor terraces.

Potential growth rate G^* has a very modest influence on the number of terraces in uplift mode, only for vertical rates over 0.5 mm/year. For such rates, minor variations of the sea level can be recorded in the sequence. In subsidence mode, increasing G^* up to 15 mm/year significantly decreases the number of preserved terraces (by a factor of ~ 2 for G^* ranging between 5 and 15 mm/year), because it sets the vertical aggradation rate and therefore controls give-up or keep-up and catch-up regimes during transgressions. At low potential growth rate, reefs are more prone to drowning, even during slower and shorter intermediary transgressions, whereas reefs with high potential growth rate are able to keep up during these minor transgressions (as MIS 3, 5b, and 7b), which cause terraces to drown only during major transgressions (as MIS 2, 6, 10, and 12).

Erosion rate has no influence on the number of terraces in uplifting sequences and a modest influence in subsident ones. During low sea level stands, abrasion platforms and erosional coastal cliffs develop, even in case sea floor is too deep for reef construction. This process forms morphological terraces unrelated to reef construction; the age of the morphology is thus different from the age of the individual corals found on their flat.

4.2. Terrace Width

In our simulations, the width of terraces is measured from the proximal break in slope initiating the terrace flat to the foot of the associated distal cliff or to the break in slope indicating the termination of the terrace fore slope. Terraces in subsiding sequences are 2 to 3 times larger than in uplifting sequences (Figure 7b). This is mainly due to the growth regime of coral reefs. Indeed, the width of a reef is primarily controlled by the geometry of its accommodation space. In subsidence mode, the accommodation space is constantly rejuvenated (as long as the reef keeps up), which makes foundations that were not covered by prior generations of reefs available to reef development. During a cycle of sea level oscillation, this mechanism allows for shoreward progradation of the reef system, while the location of the reef crest remains almost stationary (only sedimentation slightly expand the accommodation space seaward). This process lasts until the reef gives up, that is, until the rate of sea level rise exceeds the effective growth rate of the reef. The time span between two successive give up events controls the number of terraces, and is therefore an indirect control on reef width during subsidence. In the case of Hawaii (see above), the succession of *catch-up*, emergence and keep-up during reoccupations occurs over more than 100 kyr for the construction of T-1, from the fast transgression of MIS 5e to the Holocene transgression, widening the platform to several kilometers. The occasional reoccupation of earlier reef flats during transgressive events further contributes to widen the terraces. As reoccupation occurs systematically with minor transgression during subsidence, it explains the nonmonotonic evolution of the average width, as well as the important standard deviation of the width (Figure 7b). Drowned terraces are narrower for higher subsiding rates, as give up more regularly occurs.

Conversely, uplift facilitates the saturation of the accommodation space, in concert with reef construction. Reoccupation of earlier terraces more rarely occurs in uplifting sequences because they are more likely to lie above sea level and therefore to be withdrawn from the system. This in turn makes the accommodation space for uplifting sequences less variable than for subsiding sequences, both within a single sequence or for different uplift rates, which explains why the width of uplifting terraces varies less than the width of subsiding terraces.

Other second-order parameters play a role too. Initial slope α has a greater impact on the width and variability in subsidence than in uplift mode (Figure 7b, left panel). In both cases, steepest slopes ($\geq$10%) show the narrowest and least variable terraces, because the initial slope of the foundation directly controls the geometry of the accommodation space (narrow with steep slopes and wide with shallow dipping slopes). Gentle slopes then lead to the formation of more variable terraces, as they provide a larger accommodation space which may not always be completely filled up by the reef.

Potential growth rate G^* exerts a great influence on the subsiding terraces width and variability where a decreasing G^* lowers their widths. Indeed, G^* is responsible for the reef ability to keep up with sea level variations. Increasing potential growth rate enables the reef to accommodate faster transgressions, which leads to the development of wider terraces. As subsidence enables the reef to grow on the widening reef flat during successive sea level oscillations, very wide terraces (>5 km) may appear in the sequence, and width variability also increases (Figure 7b, middle panel). In uplift mode, higher values of G^* cause wider terraces, but to a smaller extent. G^* is also responsible for the ability of the reef to first keep up construction over the reef flat during transgressions and then to fill its accommodation space within the duration of the sea level stand if needed. For $G^* = 15$ mm/year, all reefs saturate the accommodation space, which explains why width variability remains consequently low. Erosion has no major impact on the width of the terraces (Figure 7b, right panel), except for low subsidence rates, which give the abrasion platform time to expand if marine erosion is efficient.

4.3. Barrier Reefs

Barriers are commonly described in subsiding reefs, but seldom mentioned are those found in uplifting coasts. They can be found as modern features, but also as fossil structures (as in the above described case of Wangi-Wangi, Figure 5, or in the Huon peninsula, as described by Chappell, 1974). In our simulations, the number of preserved barriers in uplift mode remains low (mostly less than three). Conversely, the predicted number of barriers in subsiding sequences increases with subsidence rate up to a certain extent where the number of barriers drastically decreases (Figure 7c). Shallow slopes ($\alpha \leq 2\%$) are more prone to develop and preserve barriers in both uplift and subsidence modes (Figure 7c, left panel).

These two sets of parameters (gentle slopes and subsidence) encourage the formation of wide platforms, on which reefs more efficiently develop their crests than the lagoon side, subsequently creating barriers. The potential reef growth rate G^* modulates the development of barriers, particularly in subsiding sequences: More barriers occur with lower values of G^*. Barriers develop when rates of relative sea level rise and reef growth compete, during transgressions. When the effective growth rate supersedes transgression rates, vertical aggradation of the reef is hampered by sea level, and it fills up the entire accommodation space. When growth rate is conversely too low with respect to relative sea level rise, the reef gets drowned too quickly for a barrier to develop. This explains the decreasing number of barriers during fast subsidence. There is therefore a theoretical threshold for subsidence rate, which is a linear function G^*, that prevents barriers to form. A value of 5 mm/year for G^* provides the greatest amount of barriers because many transgressions reach rates between 5 and 10 mm/year (Figure 3 ; Bintanja et al., 2005; Waelbroeck et al., 2002).

Finally, lower erosional potential E^* obviously preserves more barriers in the final sequence (Figure 7c, right panel). In uplift mode, increasing erosion rates almost completely dismantles fossil barrier reefs.

4.4. Reefal Sequences

The parametric study and the distribution of effective vertical reef aggradation (Figure 2b) indicate that the effective growth rate of coral reefs is mainly constrained by relative sea level variations. This implies that terrace morphologies adjust to the rates of relative sea level change, dictated by absolute sea level oscillations and vertical land motion. This ultimately shapes the overall architecture of reef sequences and is illustrated by the different external architectures of the sequences summarized in figure 8, where high vertical land motion rates (−1.5 and 1.5 mm/year) provide more terraces than lower vertical rates (−0.6 and 0.6 mm/year). In order to better apprehend a great number of sequences, we synthetize the morphology of sequences (number of terraces and barriers and width and height of each geomorphological feature) into barcodes, visible on the right of each sequence in figure 8.

The "Quaternary glacial cycle" is all but cyclical. Over the long term, the periods and amplitudes of the oscillations drift, to the first order, from the *40-kyr world* (amplitudes of ~60 m, periods of ~40 kyr) to the *100-kyr world* (amplitudes of ~120 m, periods of ~100 kyr) across the Mid-Pleistocene Transition (MPT). MIS 11, which shows a prominent (and most important throughout Quaternary times) episode of transgression, stand and regression, terminates the MPT (Figure 3). More precisely, all glacial cycles are also irregular and include short-lived events (like the Heinrich events or Meltwater Pulses for the most recent period). This is critical to the morphology of the reefs, that respond unevenly to the specificities of each cycle. We thus anticipate that the fingerprint of a given cycle is possibly diagnostic of the stage it belongs to. By extension, although some form of cyclicity is of course expected to the first order, the barcode that a sequence of reefs

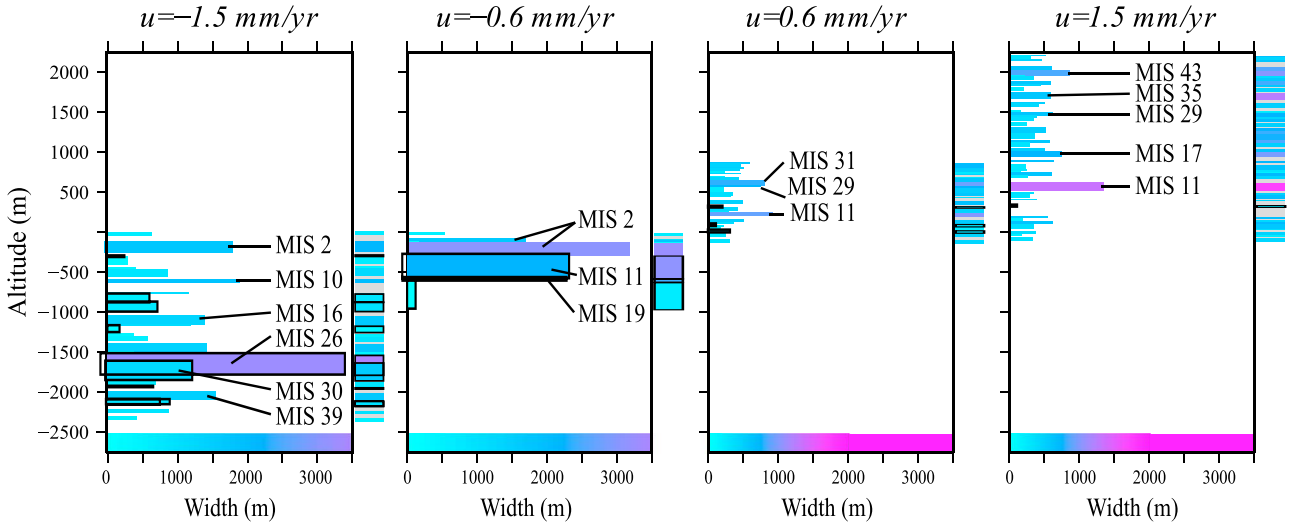

Figure 8. Modeled architectures—or *barcodes*—of two subsiding sequences (first and second panels, −1.5 and −0.6 mm/year) and two uplifting sequences (third and fourth panels, 0.6 and 1.5 mm/year). The morphology of the sequences is summarized by the relative distribution of terraces, each of them being defined by their widths (as they appear in abscissae) and heights (as revealed by the thickness of individual segments) and by the occurrence of fossil barriers (solid black outlines). The isotopic stage corresponding the last episode of reef construction on the terrace flat or barrier is indicated for prominent features. The external architecture of each sequence is synthetized into barcodes, with similar color scales for terrace width, on the right of each graph.

forms, reflecting the number and size of its terraces and the occurrence of barriers should in principle be diagnostic of the parameters that prevailed during its development.

We therefore set out to test this hypothesis by analyzing the predicted architectures—or barcodes—of our simulations. We automatically extracted the widths and heights in the final morphology of the simulations for our reference case (see parameters in Table 1), that we complement with the number of occurrence of preserved fossil barriers (Figure 9). Similarly to terrace width, terrace height is measured in this study by the difference in elevation between the proximal break in slope and the distal foot cliff or break in slope. We additionally determined the last isotopic stage associated to reef construction on the morphological flats (Figure 10). These metrics characterize the barcode of each individual sequence in a quantified manner.

4.4.1. Morphological Barcodes

The most straightforward result is the increasing number of terraces with increasing rates of vertical land motion, as already suggested by the previous analysis of particular cases, and more generally represented in Figure 7a. The increase is not linear because for absolute rates higher than ~ 0.8 mm/year, the bedrock more often outcrops, occasionally covered by a veneer of coral reef that has no significant morphological expression. There is a maximum number of terraces that can form over a time period (here 1.5 Myr), This explains why at higher rates, almost no reefal unit from former MIS is reoccupied, and most of the terraces are left isolated, separated by the raw bedrock from adjacent reef terraces or fossil barriers (see also Turcotte & Bernthal, 1984). Conversely, the bedrock seldom outcrops at low rates. The gradual appearance of the raw bedrock differs between uplift and subsidence. In uplift mode, the bedrock occasionally appears at multiple locations, the situation differs in subsidence mode, where fewer segments of raw foundations outcrop. This is explained by an equally important feature result: terraces are much higher in subsidence mode than uplift mode. While the height of the terraces seldom exceeds 50 m in uplift mode, subsiding sequences often display terraces higher than 100 m. The situation is even more critical at low rates in subsidence mode, where few high and wide terraces (several hundred meters high and several thousand meters wide) dominate the architecture of the sequences.

Another striking feature of Figure 9 is the consistency of morphological traits that dominate the barcode regardless of the vertical rates of land motion. Again the situation differs between subsidence and uplift modes. During uplift, this is best exemplified by the widest terrace, which formed during MIS 11 and forms a robust trend on the graph. Importantly, the reef terrace that finally formed during MIS 11 is essentially fringed by raw bedrock for higher vertical rates. More specifically, some MIS almost systematically develop the largest terraces, which are more than a kilometer wide, and accompanied by cliffs of a few tens of meters,

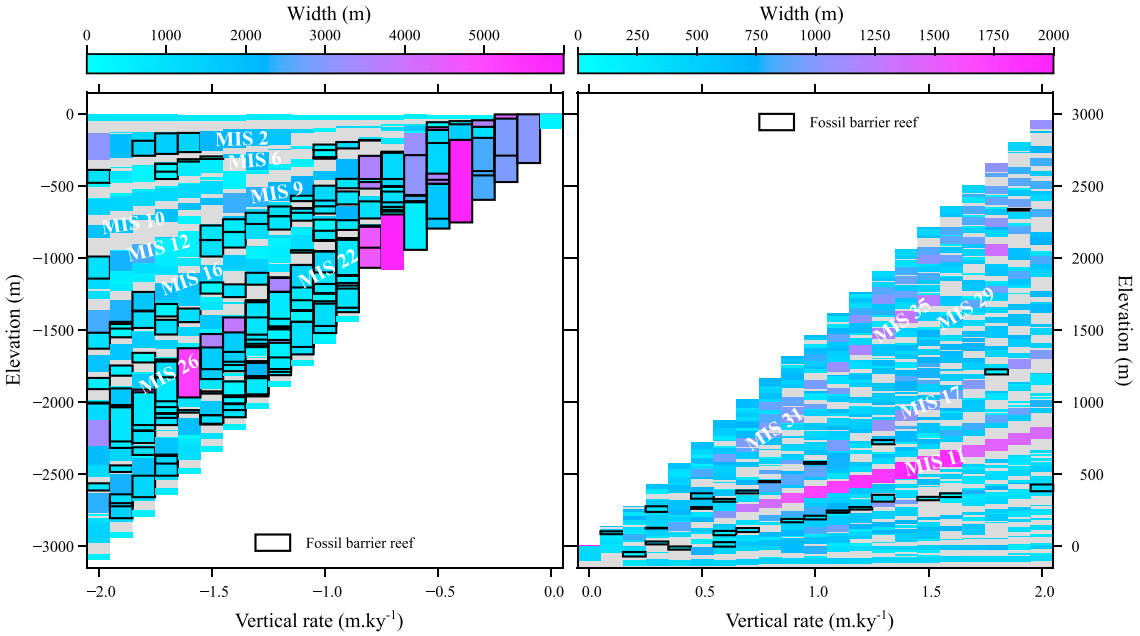

Figure 9. Modeled architectures—or *morphological barcodes*—of subsiding (left) and uplifting (right) sequences of coral reefs for a range of subsidence and uplift rates (from −2 to 0 mm/year, left; from 0 to 2 mm/year, right), as revealed by the morphology of the sequences. Terrace widths are color coded; their heights are given by the thickness of individual blocks. Solid black outlines indicate occurrences of fossil barriers. Gray areas represent the absence of any automatically detected terrace (bare foundations outcrop). Note the distinct color scales for subsidence (left) and uplift (right). All parameters but vertical rates are those of the reference case ($G^* = 10$ mm/year, $\alpha = 6\%$, $E^* = 20$ mm/year; other parameters as in Table 1).

in uplifting sequences: MIS 11 (eustatic maximum at 401 ka), MIS 17 (692 ka), and a cluster of isotopic stages between 29 and 35. The fact that the terraces that are associated with these stages trend on the global stack (Figure 9) indicate that they should be persistent geomorphological features, detectable in the landscape. MIS 11 marks the onset of high amplitude (~120 m) transgressions. Because sea level rise during MIS 11 transgression is relatively slower than other MIS transgressions (lower than 11 mm/year, cf. Figure 3) and monotonic enough for most reefs to keep-up during the transgression, it allows reefs to develop wide and thick limestone units during the transgression. However, the height and width predicted by the model for the terrace associated with this isotopic stage is not constant regarding vertical rate (cf. Figure 9). For instance, MIS 11 terrace reaches its maximum volume at uplift rates of 1.4 mm/year. During subsidence, some trends imprint the architecture too, but the signal is less clear. Trends of raw outcrop delineate the reef units finally formed during MIS 2, MIS 6, MIS 9 and 10, and MIS 12. Their height can be diagnostic too. For example, reef units formed during MIS 22 and MIS 26 form massive, several-hundred-meter-high cliffs. These should be striking features of submarine sequences.

As the sequence stretches with faster rates of vertical land motion, more terraces representing distinct MIS appear in the architecture of the sequence. Yet, the gradual inception of individual MIS units with increasing absolute vertical rates is not linear. In uplifting sequences, highstands showing the maximum elevations will appear first (MIS 5e, 11, 19, 21, 25, 31, and 37, followed by MIS 7c, 8, 9, 15, 43, etc.). In subsidence mode, the trend is less clear for lower vertical rates. Globally, the maximum accelerations of sea level rise (Figure 3), responsible for reef drowning, appear first (Holocene transgression, MIS 2, 6, 8, 16, 22, 13, and 12).

Another important feature of figure 9 is the occurrence of fossil barrier reefs. These are more frequent in subsidence mode than in uplift mode. This is explained by the fact that wider platforms develop during subsidence than during uplift, and those are more prone to develop barrier reefs. However, fossil barrier reefs are represented in uplift mode, as exemplified by our case study of Wangi-Wangi (Figure 5). Uplifted barriers often mark the reef units formed during MIS 17 and MIS 7, as supported by the two rising trends of fossil barriers on Figure 9. Besides these two episodes, uplifted barriers are very rare in our simulations. As such, they are fundamental diagnostic features in the barcodes of uplifted sequences.

In subsidence mode however, barriers are ubiquitous. Yet, some MIS are more prone to develop barrier reefs than others. While barrier reefs virtually mark all morphological units in subsiding sequences prior to MIS

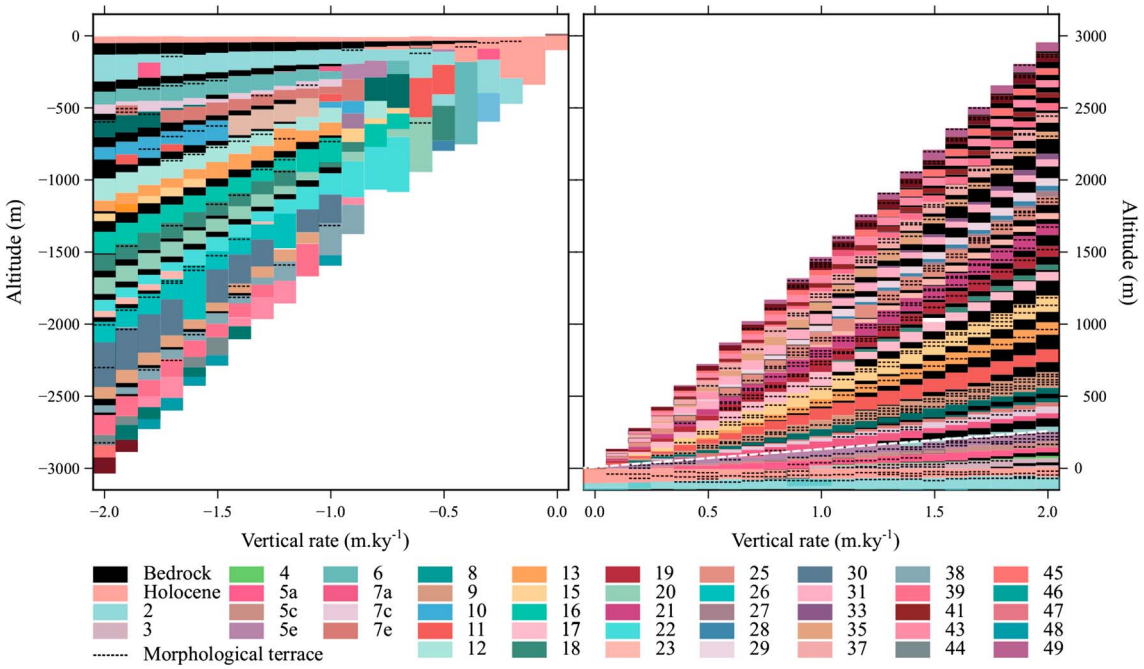

Figure 10. Modeled architectures—or *kinematic barcodes*—of subsiding (left) and uplifting (right) reefal sequences for a range of subsidence and uplift rates (from −2 to 0 mm/year, left; from 0 to 2 mm/year, right), as revealed by the last MIS of construction of terrace flats or fossil barriers prior to abandonment. Multiple terraces formed during a single cycle of eustatic variations are shown by dashed lines. All parameters but vertical rates are those of the reference case ($G^* = 10$ mm/year, $\alpha = 6\%$, $E^* = 20$ mm/year; other parameters as in Table 1). Dashed white line indicates theoretical elevation of the highstand of MIS 5e according to Waelbroeck et al. (2002). MIS = Marine Isotopic Stage.

21, they are far less frequent after MIS 11. This likely responds to the changing frequencies and magnitudes, thus rates, of sea level oscillations, prior and after the Mid Pleistocene Transition. Before MIS 11, rates of sea level rises commonly peak at slower rates (between 6 and 8 mm/year), which is close to effective reef growth rate for our reference case (Figure 2b), and thus promotes the development of barrier reefs. Conversely after MIS 11, rates of sea level rises commonly exceed 8 mm/year, which frequently leads to fast reef drowning and thus hampers the development of barrier reefs.

4.4.2. Kinematic Barcodes

Our simulations ultimately predict the morphological evolution of reefal sequences. In order to do so, our model simulates the dynamics of the active reef at all times. We take advantage of these results to unravel the mechanisms of terrace formation during sea level oscillations. The architecture of reef sequences often depart from the common assumption that each terrace represents a unique sea level highstand, and reciprocally, that all highstands are expressed as a unique terrace. Figure 10 revisits the architecture of the sequences of coral reefs (for our reference parameterization), but instead of considering their morphological barcodes, it indicates the last isotopic stage that formed a given terrace flat prior to being abandoned, as a such can be regarded as kinematic barcoding. In the following, we analyze the kinematics of terrace development during isotopic stages or substages (as defined by the time lag that separates halfway amplitudes of transgressions and regressions).

Following morphological barcodes, the contrast between subsidence and uplift modes is striking in the kinematic barcodes: During subsidence, construction prevails over eustatic variations for much longer durations, which consequently renders individual terraces larger. The contrast between uplift and subsidence modes is also revealed by the period of a cycle (transgression, regression, sea level stands) during which terraces are last constructed: While in uplift mode, the last episode of construction of terraces is dominated by sea level highstands (odd-numbered MIS, warm colors on Figure 10), in subsidence mode, these episodes are dominated by fast transgressions, often occurring during glacial periods (even numbers, cold colors on Figure 10). The explanation is straightforward in uplift mode, where sea level highstands often mark the last episode of reef growth prior to emersion caused by regressions and uplift. In subsidence, the fact that glacial isotopic stages dominate the barcode implies that reef construction continues during regressions and lowstands, and

that reef flats are drowned and abandoned during subsequent transgressions, when the rate of sea level rise supersedes the maximum effective growth rate. These peaks of acceleration of sea level rise are commonly found in the first part of the transgression.

An important result that may echo field observations is the fact that some sea level stands (either high or low stands), although prominent in the sea level curve, are occasionally unrepresented in the final architecture of a sequence. For instance, in our reference case and for vertical rates of 0.4 and 0.5 mm/year, no terrace is capped by reef construction associated with MIS 7c, although its highstand culminates at −4 m according to Waelbroeck et al. (2002). This is due to the unfavorable geometry of the accommodation space during sea level highstand. Detailed analysis of the sequence of construction reveals an incidental cliff down to depths larger than typical depths of reef growth (20 m in our reference case). In this case, given the chosen ASL curve, the preceding MIS 8c and 7e already saturated the accommodation space. The narrow fringing reef, which managed to keep up with the transgression is further eroded by wave erosion during the following regression and the next highstand. This example outlines the importance of uncommon settings that may preclude the expression of some sea level stands. Importantly, this observation challenges the idealized kinematic barcode, wherein each sea level stand is expressed.

Conversely, some MIS are occasionally over represented, and feature more than a single terrace. This is visible in figure 10, where dashed lines point to the elevations of multiple morphological terraces that have been constructed over a unique isotopic stage (e.g., MIS 2) or substage (e.g., MIS 5e). These occurrences are much more frequent in uplift mode than in subsidence mode. In uplifting sequences, some MIS generally exhibit several terraces for vertical land motion rates exceeding 0.6 mm/year: this is particularly true for MIS 5e, 9, 13, 15, 19, 21, 25, and 37. In subsidence, this is well exemplified by MIS 6, 10, and 26. Similarly to the absence of sea level stands, the overrepresentation of a unique MIS in multiple terraces is at odds with the commonly used interpretation of sequences of marine terraces. This *discrete* interpretation implicitly defines a bijective relationship between individual terrace and sea level stands. This assumption breaks down in many simulations. A variety of reasons explains this departure: minor events, that could be thought of as noise, actually trigger short lived episodes of backstepping of the reef. This leads to the formation of intermediate terraces. This is for example the case for MIS 13 and 15. Reoccupation of an antecedent staircased morphology during a transgression can also prevent the reef to completely fill up its accommodation space and lead to a partial drowning of the reef not necessarilly accompanied by a reef backstepping. Finally, some transgressions exhibit several peaks in the rate of sea level rise (typically MIS 5e, Figure 3), which can lead to the drowning of the reef. In subsidence mode, gradual change in relative sea level change can also switch modes between catch-up, give-up, and keep-up. The morphological expression is that of multiple terraces for a single MIS. It implies that some well developed morphological terraces in the sequence are not associated with any sea level stagnation.

Last, as already proposed by Bard, Jouannic, et al. (1996), our model shows that a single feature can be the result of several cycles. Reoccupations are common, either superimposing additional reefal units conformably to the antecedent or just adding a thin layer of limestone. The vagaries of sea level rise can explain these occasional reoccupation of an antecedent staircased morphology, developed over preceding cycles. Generally, it promotes the development of a reef veneer on earlier terrace flats. This process is also visible in our simulations during MIS 5e transgression, for instance. At low rates (<0.9 mm/year), MIS 5e transgression reoccupies the terraces that formed during the substages of MIS 7, while for higher rates (>1.4 mm/year), the MIS 5e reef reoccupies the terraces associated with MIS 6.

Overall, the variable fingerprints of MIS thus not only respond to the properties of a given cycle of eustatic variations only (rate of sea level variations, amplitude and duration) but is also modulated by the morphology of the foundations, that is, the volume and geometry of the accommodation space. This may lead to successive reoccupations, overrepresentations of some cycles, or the absence thereof. Kinematic barcoding of numerical sequences explain why the commonly assumed bijective relationship between terraces and sea level highstands often breaks down, and that a variety of alternative behaviors jeopardizes it.

5. Discussion

Our analysis of the results of our numerical simulations indicates that few forcings are capable to shape individual reef terraces, as well as the architecture of reefal sequences. These parameters are geological forcings, and as such provide explanations for the variety of observed behaviors that are expandable as general laws.

Yet, if they are sufficient to explain the variability of architectures of reefal sequences, regardless of other environmental processes, it does not imply that the impact of local intrinsic forcings, mostly of ecosystemic nature, shall be discarded. It rather implies that geological factors more universally control the diversity of reefs systems. Our results are robust because we opted for a parametric analysis, which browses ranges of values, which limits the risk to yield predetermined results. The consequences are multiple, and we discuss a few prominent ones below.

5.1. On the Architecture of Reefal Sequences

Amongst the four parameters that we have investigated (namely vertical land motion rate U, reef growth potential G^*, erosion power E^* and initial slope α), our parametric study points to rates of vertical land motion as the main control on the architecture of reefal sequences. They set the number, width and height of individual terraces, the occurrence of barrier reefs as well as the final age of construction of a terrace flat. Surprisingly, initial slope is revealed to be the second most influent parameter. Yet, this parameter is mainly taken into account regarding terraces width (Webster et al., 2007) but seldom taken into account as a main factor, notably regarding reef growth rate (Toomey et al., 2013). Potential reef growth rate is mostly influent on subsiding sequences, while wave erosion rate efficiently controls the number of barrier reefs. Erosion also slightly impacts the terrace width for low subsidence rates and the number of terraces for high subsidence rate, but is otherwise a secondary parameter.

Of course, the accommodation space is ultimately the underlying factor, as it modulates reef growth and type (Dullo, 2005; Husson et al., 2018; Woodroffe & Webster, 2014) and directly relates to eustatic variations, rates of vertical land motion, and initial slope. For instance, steepest slopes provide narrowest accommodation spaces, that more easily gets saturated, while shallow dipping slopes tend to produce wide platforms, which can provide favorable foundations for reef growth during subsequent reoccupations, as well as large accommodation spaces.

More importantly, vertical land motion is crucial. During subsidence, while the reef keeps up, wide platforms develop and the accommodation space broadens. Subsidence constantly expands the accommodation space during sea level stands, while uplift conversely expedites the closure of the accommodation space. Of course, these rules may break down. For instance, subsidence occasionally creates unfavorable geometries, as sea level often meets steep fore reef slopes or cliffs during the last stages of regressions, which prevent reef construction. These periods of reef dormancy can last up to 50 kyr. This contrasted regimes yield a great variability of terraces width within a sequence but also a great variability in reef productivity Husson et al. (2018). In uplift mode, transgressions often lead to reoccupations of former terraces, yielding narrow accommodation spaces and more unfavorable geometries than bare foundations, which are only met during major regressions. The accommodation space is thus less variable through eustatic variations during uplift than during subsidence, which induces a more constant productivity of the reef with fewer and shorter periods of quiescence of the reef.

Potential reef growth rate is a secondary parameter, whose influence is only expressed when the reef is challenged by a sudden increase of the accommodation space. In our simulations, such events are rare and mainly occur during fast transgressions reoccupying wide platforms. They are preferentially found in subsidence mode, which explains why the influence of potential reef growth rate is more clearly expressed in subsiding sequences. The remarkable distribution of effective reef growth rates (as in Figure 2b), that systematically minor the potential reef growth rate to lower values, shows that the accommodation space hampers reef growth before the potential reef growth rate may significantly restrict the development of coral reefs.

In our parametric study, erosional potential seems to have negligible impact on the architecture of reef sequences. In fact, wave erosion has counterbalancing effects: wave erosion undermines cliffs and can erase earlier generations of terraces, but simultaneously broadens the active reef flat (Figure 3 in Pedoja et al., 2018), which will be subsequently reduced by the same process, after its emersion. Regarding the overall morphology of reef sequences, wave erosion and subsequent sedimentation smoothens the topography by diffusion over the active reef fore slope, and conversely sharpens the earlier reef terraces. Although its incidence on the architecture of reefal sequences is minor (with respect to vertical land motion or initial slope), it has a noticeable impact on the development of composite terraces, where markers of different MIS can coexist on a unique reef flat. Composite terraces are ultimately shaped by the last episode of sea level stagnation, during which wave erosion levels down small differences of elevations between the former and currently

constructed reefal unit. Although it marginally impacts the final architecture of the reef sequence, it is certainly primordial when attempting to assign ages to terraces. This conclusion corroborates the previous work of, for instance, Bard, Jouannic, et al. (1996), Chappell et al. (1996), and Speed and Cheng (2004).

Last, stochasticity, as expressed for instance by the short-term vagaries of relative sea level change and the irregularity of all processes at play, increases the variability of the accommodation space. For instance, unfavorable geometries can lead to the absence of reef construction during a eustatic cycle (e.g., MIS 7c). On the opposite, an excessively broad accommodation space can lead to the reef backstepping, and therefore to several slope breaks and ultimately multiple terraces (e.g., MIS 5e). Similarly, irregular foundations can also develop several morphological flats during a single isotopic stage.

5.2. On the Genesis of Barrier Reefs

Our model gives new insights on the variability of reef types, herein on the distribution of fringing and barrier reefs. Common theories either assign a prime role to subsidence (e.g., Darwin, 1842), or to eustatic variations that shape wide platforms during glacial stages (e.g., Daly, 1915). Blanchon et al. (2014) proposed that the reoccupation of subsiding former flats during transgressions initiates barrier reefs. Importantly, these mechanisms are irrelevant for the seldom described uplifted barriers. Both the example of Wangi-Wangi (see section 3.2) and our parametric study (see section 4.3) reveal that the joint effects of eustatic variations and uplift can also lead to favorable conditions for the development of barrier reefs in uplift mode.

On this basis, one can derive systematic behavior laws for the formation and preservation of barrier reefs. According to our simulations, barrier reefs initiate in narrow parametric windows combining a wide accommodation space (because barrier reefs more easily nucleate on the distal edge of wide platforms or very shallow dipping slopes) and a fine competition between the rate of relative sea level change and the reef growth rate. These conditions should be met to allow for the reef crest to grow at a maximal rate, that is, approaching G^* as much as possible. This competition occurs in our simulation of Wangi-Wangi during the transgression preceding MIS 7e, for a maximum rate of sea level rise of ~14 mm/year, slightly higher than the effective reef growth rate of ~11 mm/year. Once the barrier nucleates at the reef crest, the increase of the water depth over the former reef flat during transgressions, to a value close to the maximum depth for reef construction, more easily prevents the reef to keep-up along the whole reef flat, but fosters the further development of the shallower reef crest that grows along with sea level rise and forms a barrier. The absence of barrier reefs in the Hawaiian sequence can be explained by the high rate of subsidence, the moderate reef growth rate, and the large depth of reef construction. Major and fast transgressions lead to the sudden drowning of the reef as the rate of sea level rise combined to the fast subsidence (i.e., ~28 mm/year for MIS 5e) supersedes the effective growth rate of the reef (~5 mm/year). On the opposite, minor and slow transgressions (i.e., ~9.5 mm/year for the relative sea level rise during MIS 5a) only reoccupy the former platform, providing a water depth too shallow to express a sufficient gradient in reef growth along the reef flat to initiate a barrier reef.

Once initiated, the barrier can keep up with sea level rise, while the lagoon more easily gives up. The process may take place over several successive eustatic cycles, as revealed in many simulations, including uplifting sequences, as well illustrated by that of Wangi-Wangi (Figure 5). Of course, this mechanism applies to subsiding regions, where the polygenic construction of barriers, or at least their foundations of Pleistocene age or older, is documented in many areas, such as Tahiti (Bard, Hamelin, et al., 1996; Blanchon et al., 2014), Mururoa (Camoin et al., 2001), or the Great Barrier Reef (Braithwaite & Montaggioni, 2009).

The lateral variability of the slope could explain, along with the distribution of wind and consequent waves, the variability of the morphology of the modern reef, for instance at Tahiti, where the modern barrier reef is found on the most gentle slopes of the island. Conversely, the lateral variability of the modern reef on the northern and eastern sides of Wangi-Wangi, where slopes are more uniform, is correlated with the dip of the emerged terraces, and is thus possibly related to variations in the vertical rate.

Last, fossil barrier reefs need to resist to sea level erosion, which limits the preservation of barriers in the sequence, especially during subsequent regressions. Erosion reinforces the numeral difference of occurrence of barriers between uplifting and subsiding regimes, because subsidence more easily prevents sea level erosion to reach the base of the barrier during the following regression. Conversely, uplifting barriers are more likely to be exposed to shallow sea levels during the following transgressions, and thus be completely

eroded. Indirectly, the fact that they remain as fossil barriers in places like Wangi-Wangi bounds the values of erosional potential E^*, for large values of E^* yield to the erasure of earlier barriers.

Overall, the fine parameterization of four processes give rise to barrier reefs, regardless of the subsidence or uplift of the sequence: optimal competition between reef growth and sea level rise rates, wide platforms, preservation from wave erosion, and reoccupation. However, because, the appropriate conjunction of these parameters is more commonly associated with subsidence, it explains the greatest occurrence of barriers in subsiding coasts than in uplifting ones, but with a unique mechanism.

5.3. Toward a Continuous Interpretation of Reef Sequences

A profound outcome of this meta-analysis is that it invites for a revision of the simplified paradigm of the discrete approach, where each terrace is assigned to a unique sea level highstand, and reciprocally. In that sense, our results may alleviate the mounting paradox that arises from the increasing numbers of available datings and documented sequences. Observations reveal the diversity in the architecture of sequences, and departure from the bijective relationship between sea level stands and morphological units, or reef terraces, are commonly reported: composite terraces where several reefal units from different MIS are represented (Barbados: Speed & Cheng, 2004; Sumba: Bard, Jouannic, et al., 1996; Ular: Pedoja et al., 2018), corals dated from a unique MIS on different morphological levels (Haïti: Dumas et al., 2006, Sumba: Bard, Jouannic, et al., 1996), absence of MIS (Wangi-Wangi), etc. Similarly, the discrete approach assumes that coral reefs mainly grow during sea level stands. Again, this is at odds with observations that reveal that coral reefs grow at their fastest rates during transgressions (e.g., Blanchon et al., 2014; Cabioch, 2003; Dullo, 2005; Leclerc et al., 2015). Our analysis shows that departure from the discrete approach is in fact commonplace and provides the theoretical grounds to understand these observations. Such deviations from the theory are commonly interpreted in terms of local idiosyncrasies (sedimentary flux, hydrodynamics, coseismic uplift, or subsidence, etc.). Based on our parametric study, we contend that they can be explained by a unified theory. Vertical land motion or initial slope tweak reef growth rates in a way that can consistently generate such features, regardless of other environmental specificities (although they should not be ruled out, of course). We emphasize that a more dynamic and continuous view, in which reef expansion is constrained by relative sea level oscillations (Dullo, 2005; Woodroffe & Webster, 2014; Husson et al., 2018), should replace the discrete approach.

In this framework, the continuous interplay between reef growth, erosion and sedimentation during sea level oscillations implies that reef terraces are not necessarily associated to sea level stands, that terraces can develop during several cycles of sea level oscillations, and terrace surfacing is achieved over multiple eustatic cycles. Similarly, the internal architecture of the sequences is made of reefal units that are often constructed during multiple cycles. Such behaviors are most common at moderate rates of uplift or subsidence. Overall, this implies that terraces are characterized by several ages: one for each episode of construction, if any; one for the final episode of drowning or emergence; and possibly one for the last episode of erosion. The resulting distribution of ages within a sequence prevents a straightforward interpretation of the age-elevation relationship, typically for tectonic purposes, unless uncertainties are computed accordingly, and therefore increased to alarming values.

5.4. Implications for Eustatic Reconstructions and Uplift Rates Estimates

These results imply that inverting sea level oscillations from flights of coral reefs is more complex than from erosional terraces. When uplifted, the altitude of a given terrace neither precisely matches the associated maximum sea level stand, nor its age, because the reef flat is generally last shaped during the beginning of the regression due to down leveling by marine erosion. These behaviors are often visible in our simulations for MIS 5e, whose theoretical final altitude (indicated by the white dashed line in figure 10) is regularly higher than the highest terrace associated with this isotopic stage. A striking example occurs for a vertical land motion rate of 1.4 mm/year, for which the altitude of the uppermost MIS 5e terrace is ~15 m lower than the theoretical elevation of the highstand. This process impacts eustatic reconstructions in two ways. First, it lowers the purported elevation of the former reef flat by a few meters, leading to a possible underestimation of the elevation of the highstand. Second, it jointly exposes reefal units built at the end of the transgression and at the beginning of the regression, yielding an apparent range of ages for many terraces, as in Bard, Jouannic, et al. (1996). These effects can be reinforced in some cases because of the observed (Kemp & Sadler, 2014) or theoretical (Husson et al., 2018) delays of a few kiloyears between maximal aggradation rates and acceleration of sea level changes.

Finally, the morphology of a given terrace (width and height, thus its importance within a sequence) can be misleading, for is not necessarily related to the amplitude of the associated transgression. Major transgression can leave tenuous fingerprints (as for MIS 5e), while more moderate ones can form significant stable features (as for MIS 29). The variability of the width and height of a reef terrace is once again strongly constrained by the geometry of the accommodation space. This is well illustrated by the variability of the dimensions of the uplifting terrace finally constructed during MIS 11, whose maximum width and height are found for a vertical rate of 1.5 mm/year (Figure 9).

6. Conclusions

We devised a numerical model that can be used to unravel the architecture and genesis of reefal sequences. This tool successfully reproduces the observed morphologies of reef sequences and is in good agreement with previous models (Toomey et al., 2013; Webster et al., 2007). We extracted from the simulations the number, width and height of individual reef terraces, along with the reef type (fringing or barrier) within a sequence, which gives insights on the genesis, growth and architecture of coral reefs. Importantly, as any model which is calibrated on observations, it allows to expand the knowledge to domains that are unaccessible on the sole basis of observations. We took advantage of this approach to go beyond the reproduction of observations, and to explore the behavior of coral reefs, when exposed to variable sets of parameters. This approach complements data compilations to extract general laws that can be generalized, which is seldom done for reefal sequences.

Our parametric study permits to extract general laws. In order to simultaneously analyze the many simulations that serve as our database, we extract a few metrics to characterize the geometry and architecture of reefal sequences. When concatenated, it appears that these metrics barcode the sequences of coral reefs. It therefore invites to systematically describe natural sequences from field observations in a similar fashion. In theory, that should almost suffice to retrieve the parameterization of a given sequence (U, G^*, E^*, and α), by confronting it to our database of barcodes. In practice, because sequences in the field can often be incompletely documented, or because local processes add enough noise to blur the signal, we anticipate that this operation can not be done automatically. However, provided it is completed by a manual control, this inversion should suffice to bracket a range of parameters at first order.

One main outcome is that extrinsic, geological forcings, are prominent factors, and suffice to explain the main traits of reefal sequences. Our analysis confirms that vertical land motion is the main factor influencing the development of coral reefs (e.g., Husson et al., 2018; Toomey et al., 2013), followed by the slope of the foundations. The growth rate of the reef itself only modulates it to a minor extent. Erosion plays a role that can be important to specific aspects; reef type is efficiently controlled by erosion.

Importantly, we quantitatively demonstrate—perhaps for the first time—how barrier reefs, that are generally thought off as archetypical of subsiding domains, can also be present in uplifting regions. These features are found, for instance, in eastern Indonesian islands, like Wangi-Wangi, and are well reproduced in our simulations. Because the parametric windows that permit their development are narrower in uplift mode than in subsidence, uplifting sequences are less likely to display such features, both for the modern reef and their fossil, uplifted counterparts. Interestingly, because these windows are narrow, they can serve as precise sensors to invert for the parameters that prevail in a given sequence. The initiation of barrier reefs provides crucial insights not only on the potential growth rate of a reef, seldom expressed along eustatic variations, but also on the distribution of the initial slope, vertical land motion, and erosion rate.

These multiple simulations also illustrate the non linearity in the behavior of reefs. If some episodes during their Quaternary evolution consistently stand out (like the overwhelming development of massive coral reef terraces during MIS 11, 17, or 31), sequences often depart from a systematic distribution of reefal units, stacked according to their age distribution. In an nonintuitive manner, our simulations show that some stages of sea level oscillations might be overrepresented as multiple reef terraces or barriers, some might be absent, and several cycles may be found at similar elevations in composite terraces. Consequently, dated terraces surfaces should be interpreted with great caution for eustatic reconstructions and vertical motion rates estimates. Reefal sequences should not be considered as stacks of independently built coral reef terraces, constructed over individual episodes, but as a continuous construction, chiefly dictated by the variations of the accommodation space. At the scale of a reef terrace, the possibility of polycyclic history highlight the need of multiple datings on a terrace flat.

Acknowledgments
We thank the State Ministry of Research and Technology of Indonesia "RISTEK" that allowed us to conduct the field trip to Sumba (research permit 680/FRP/E5/Dit.KI/IV/2017). We thank ANR jcjc program GiSeLE for funding the initiation of this study. We also thank Johan Andersen for his logisitcs and support in the field. The code can be downloaded from the supporting information repository.

References

Agassiz, A. (1903). *The coral reefs of the Maldives* (vol. 29). Cambridge, USA, University of Harvard: Museum of Comparative Zoology at Harvard College.

Anderson, R. S., Densmore, A. L., & Ellis, M. A. (1999). The generation and degradation of marine terraces. *Basin Research*, *11*(1), 7–19. https://doi.org/10.1046/j.1365-2117.1999.00085.x

Andréfouët, S., Cabioch, G., Flamand, B., & Pelletier, B. (2009). A reappraisal of the diversity of geomorphological and genetic processes of New Caledonian coral reefs: A synthesis from optical remote sensing, coring and acoustic multibeam observations. *Coral Reefs*, *28*(3), 691–707. https://doi.org/10.1007/s00338-009-0503-y

Bard, E., Hamelin, B., Arnold, M., Montaggioni, L., Cabioch, G., Faure, G., & Rougerie, F. (1996). Deglacial sea-level record from Tahiti corals and the timing of global meltwater discharge. *Nature*, *382*(6588), 241.

Bard, E., Jouannic, C., Hamelin, B., Pirazzoli, P., Arnold, M., Faure, G., et al. (1996). Pleistocene sea levels and tectonic uplift based on dating of corals from Sumba Island, Indonesia. *Geophysical Research Letters*, *23*(12), 1473–1476. https://doi.org/10.1029/96GL01279

Barrett, S. J., & Webster, J. M. (2012). Holocene evolution of the Great Barrier Reef: Insights from 3D numerical modelling. *Sedimentary Geology*, *265-266*, 56–71. https://doi.org/10.1016/j.sedgeo.2012.03.015

Bintanja, R., van de Wal, R. S. W., & Oerlemans, J. (2005). Modelled atmospheric temperatures and global sea levels over the past million years. *Nature*, *437*, 125.

Blanchon, P., Granados-Corea, M., Abbey, E., Braga, J. C., Braithwaite, C., Kennedy, D. M., et al. (2014). Postglacial fringing-reef to barrier-reef conversion on Tahiti links Darwin's reef types. *Scientific Reports*, *4*, 4997–5005. https://doi.org/10.1038/srep04997

Bosscher, H., & Schlager, W. (1992). Computer simulation of reef growth. *Sedimentology*, *39*(3), 503–512. https://doi.org/10.1111/j.1365-3091.1992.tb02130.x

Braithwaite, C. J. R. (2016). Coral-reef records of Quaternary changes in climate and sea-level. *Earth-Science Reviews*, *156*, 137–154. https://doi.org/10.1016/j.earscirev.2016.03.002

Braithwaite, C. J., & Montaggioni, L. F. (2009). The great barrier reef: A 700 000 year diagenetic history. *Sedimentology*, *56*(6), 1591–1622.

Cabioch, G. (2003). Postglacial reef development in the South-West Pacific: Case studies from New Caledonia and Vanuatu. *Sedimentary Geology*, *159*(1), 43–59. https://doi.org/10.1016/S0037-0738(03)00094-0

Camoin, G., Ebren, P., Eisenhauer, A., Bard, E., & Faure, G. (2001). A 300 000-yr coral reef record of sea level changes, Mururoa Atoll (Tuamotu Archipelago, French Polynesia). *Palaeogeography, Palaeoclimatology, Palaeoecology*, *175*(1-4), 325–341.

Camoin, G. F., & Webster, J. M. (2015). Coral reef response to Quaternary sea-level and environmental changes: State of the science. *Sedimentology*, *62*(2), 401–428. https://doi.org/10.1111/sed.12184

Caputo, R. (2007). Sea-level curves: Perplexities of an end-user in morphotectonic applications. *Global and Planetary Change*, *57*(3–4), 417–423. https://doi.org/10.1016/j.gloplacha.2007.03.003

Chappell, J. (1974). Geology of coral terraces, Huon Peninsula, New Guinea: A study of Quaternary tectonic movements and sea-level changes. *Geological Society of America Bulletin*, *85*(4), 553–570. https://doi.org/10.1130/0016-7606(1974)85h553:GOCTHPi2.0.CO;2

Chappell, J. (1980). Coral morphology, diversity and reef growth. *Nature*, *286*(5770), 249.

Chappell, J., Omura, A., Esat, T., McCulloch, M., Pandolfi, J., Ota, Y., & Pillans, B. (1996). Reconciliation of late Quaternary sea levels derived from coral terraces at Huon Peninsula with deep sea oxygen isotope records. *Earth and Planetary Science Letters*, *141*(1–4), 227–236. https://doi.org/10.1016/0012-821X(96)00062-3

Crabbe, M. J. C., Wilson, M. E. J., & Smith, D. J. (2006). Quaternary corals from reefs in the Wakatobi Marine National Park, SE Sulawesi, Indonesia, show similar growth rates to modern corals from the same area. *Journal of Quaternary Science*, *21*(8), 803–809. https://doi.org/10.1002/jqs.1001

Daly, R. A. (1915). The glacial-control theory of coral reefs, *Proceedings of the American Academy of Arts and Sciences* (Vol. 51, pp. 157–251). Cabridge, USA: American Academy of Arts & Sciences.

Dana, J. D. (1885). Origin of coral reefs and islands. *American Journal of Science*, *30*(176), 89–105.

Darwin, C. R. (1842). *The structure and distribution of coral reefs, being the first part of the geology of the voyage on the Beagle, under the command of Capt. Fitzroy, R.N., during the years 1832 to 1836*, pp. 214p. London: Smith Elder and Co.

Dullo, W.-C. (2005). Coral growth and reef growth: A brief review. *Facies*, *51*(1), 33–48. https://doi.org/10.1007/s10347-005-0060-y

Dumas, B., Hoang, C. T., & Raffy, J. (2006). Record of MIS 5 sea-level highstands based on U/Th dated coral terraces of Haiti. *Quaternary International*, *145–146*, 106–118. https://doi.org/10.1016/j.quaint.2005.07.010

Fortuin, A. R., De Smet, M. E. M., Hadiwasastra, S., Van Marle, L. J., Troelstra, S. R., & Tjokrosapoetro, S. (1990). Late Cenozoic sedimentary and tectonic history of south Buton, Indonesia. *Journal of Southeast Asian Earth Sciences*, *4*(2), 107–124. https://doi.org/10.1016/0743-9547(90)90010-

Hibbert, D. F., Rohling, E. J., Dutton, A., Felicity, H. W., Chutcharavan, P. M., Zhao, C., & Tamisiea, M. E. (2016). Coral indicators of past sea-level change: A global repository of U-series dated benchmarks. *Quaternary Science Reviews*, *145*, 1–56. https://doi.org/10.1016/j.quascirev.2016.04.019

Huppert, K. L., Royden, L. H., & Perron, J. T. (2015). Dominant influence of volcanic loading on vertical motions of the Hawaiian Islands. *Earth and Planetary Science Letters*, *418*, 149–171. https://doi.org/10.1016/j.epsl.2015.02.027

Husson, L., Pastier, A.-M., Pedoja, K., Elliot, M., Paillard, D., Authemayou, C., et al. (2018). Reef carbonate productivity during Quaternary sea level oscillations. *Geochemistry, Geophysics, Geosystems*, *19*, 1148–1164. https://doi.org/10.1002/2017GC007335

Kemp, D. B., & Sadler, P. M. (2014). Climatic and eustatic signals in a global compilation of shallow marine carbonate accumulation rates. *Sedimentology*, *61*(5), 1286–1297. https://doi.org/10.1111/sed.12112

Kennedy, D. M., & Woodroffe, C. D. (2002). Fringing reef growth and morphology: A review. *Earth-Science Reviews*, *57*(3), 255–277. https://doi.org/10.1016/S0012-8252(01)00077-0

Koelling, M., Webster, J. M., Camoin, G., Iryu, Y., Bard, E., & Seard, C. (2009). SEALEX—Internal reef chronology and virtual drill logs from a spreadsheet-based reef growth model. *Global and Planetary Change*, *66*(1–2), 149–159. https://doi.org/10.1016/j.gloplacha.2008.07.011

Kuenen, P. H. (1933). The formation of the atolls in the Toekang-Besi-group by subsidence, *Proc. Kon. Akad. Wetensch* (Vol. 36, pp. 331–336). Amsterdam.

Lea, D. W., Martin, P. A., Pak, D. K., & Spero, H. J. (2002). Reconstructing a 350 ky history of sea level using planktonic Mg/Ca and oxygen isotope records from a Cocos Ridge core. *Quaternary Science Reviews*, *21*(1–3), 283–293. https://doi.org/10.1016/S0277-3791(01)00081-6

Leclerc, F., Feuillet, N., Perret, M., Cabioch, G., Bazin, S., Lebrun, J.-F., & Saurel, J. M. (2015). The reef platform of Martinique: Interplay between eustasy, tectonic subsidence and volcanism since Late Pleistocene. *Marine Geology*, *369*, 34–51. https://doi.org/10.1016/j.margeo.2015.08.001

Ludwig, K. R., Szabo, B. J., Moore, J. G., & Simmons, K. R. (1991). Crustal subsidence rate off Hawaii determined from $^{234}U/^{238}U$ ages of drowned coral reefs. *Geology*, *19*(2), 171–174. https://doi.org/10.1130/0091-7613(1991)019<0171:CSROHD>2.3.CO;2

MBARI Mapping Team (2000). MBARI Hawaii multibeam survey. *Monterey Bay Aquarium Research Institute Digital Data Series*, *2*, 2.

Medina-Elizalde, M. (2013). A global compilation of coral sea-level benchmarks: Implications and new challenges. *Earth and Planetary Science Letters*, *362*, 310–318.

Montaggioni, L. F. (2005). History of Indo-Pacific coral reef systems since the last glaciation: Development patterns and controlling factors. *Earth-Science Reviews*, *71*(1-2), 1–75.

Montaggioni, L. F., Borgomano, J., Fournier, F., & Granjeon, D. (2015). Quaternary atoll development: New insights from the two-dimensional stratigraphic forward modelling of Mururoa Island (Central Pacific Ocean). *Sedimentology*, *62*(2), 466–500. https://doi.org/10.1111/sed.12175

Montaggioni, L. F., & Braithwaite, C. J. R. (2009). *Quaternary coral reef systems: History, development processes and controlling factors*. Amsterdam, Boston: Elsevier.

Moore, J. G., & Fornari, D. J. (1984). Drowned reefs as indicators of the rate of subsidence of the island of Hawaii. *The Journal of Geology*, *92*. https://doi.org/10.1086/628910

Moore, J. G., Normark, W. R., & Szabo, B. J. (1990). Reef growth and volcanism on the submarine southwest rift zone of Mauna Loa, Hawaii. *Bulletin of Volcanology*, *52*(5), 375–380. https://doi.org/10.1007/BF00302049

Neumann, A. C., & Macintyre, I. (1985). Reef response to sea level rise: Keep-up, catch-up, give-up, *Proceedings of the Fifth International Coral Reef Congress* (vol. 3, pp. 105–110). Tahiti: Antenne Museum-EPHE.

Nunn, P. D. (1999). Late Cenozoic emergence of the islands of the northern Lau-Colville Ridge, southwest Pacific. *Geological Society, London, Special Publications*, *146*(1), 269–278. https://doi.org/10.1144/GSL.SP.1999.146.01.16

Pandolfi, J. M., & Jackson, J. B. C. (2006). Ecological persistence interrupted in Caribbean coral reefs. *Ecology Letters*, *9*(7), 818–826. https://doi.org/10.1111/j.1461-0248.2006.00933.x

Pedoja, K., Husson, L., Bezos, A., Pastier, A.-M., Imran, A. M., Arias-Ruiz, C., et al. (2018). On the long-lasting sequences of coral reef terraces from SE Sulawesi (Indonesia): Distribution, formation, and global significance. *Quaternary Science Reviews*, *188*, 37–57. https://doi.org/10.1016/j.quascirev.2018.03.033

Pedoja, K., Husson, L., Johnson, M. E., Melnick, D., Witt, C., Pochat, S., et al. (2014). Coastal staircase sequences reflecting sea-level oscillations and tectonic uplift during the Quaternary and Neogene. *Earth-Science Reviews*, *132*, 13–38. https://doi.org/10.1016/j.earscirev.2014.01.007

Sarr, A-C., Husson, L., Sepulchre, P., Pastier, A.-M., Pedoja, K., Elliot, M., et al. (2019). Subsiding Sundaland. *Geology*, *47*(2), 119–122.

Satyana, A. H., & Purwaningsih, M. E. (2011). *Collision of microcontinents with eastern Sulawesi: Records from uplifted reef terraces and proven-potential petroleum plays*. Jakarta, Indonesia: Indonesian Petroleum Association.

Speed, R. C., & Cheng, H. (2004). Evolution of marine terraces and sea level in the last interglacial, Cave Hill, Barbados. *Geological Society of America Bulletin*, *116*(1-2), 219–232.

Tomascik, T., Mah, A. J., Nontji, A., & Moosa, M. K. (1997). *The ecology of Indonesian seas*. Oxford: Periplus Editions.

Toomey, M., Ashton, A. D., & Perron, J. T. (2013). Profiles of ocean island coral reefs controlled by sea-level history and carbonate accumulation rates. *Geology*, *41*, 731–734.

Turcotte, D. L., & Bernthal, M. J. (1984). Synthetic coral-reef terraces and variations of Quaternary sea level. *Earth and Planetary Science Letters*, *70*(1), 121–128. https://doi.org/10.1016/0012-821X(84)90215-2

Verbeek, R. D. M. (1908). Molukken verslag. *Jaarboek van het Mijnwezen*, *37*, 1–826.

Waelbroeck, C., Labeyrie, L., Michel, E., Duplessy, J. C., McManus, J. F., Lambeck, K., et al. (2002). Sea-level and deep water temperature changes derived from benthic foraminifera isotopic records. *Quaternary Science Reviews*, *21*(1–3), 295–305. https://doi.org/10.1016/S0277-3791(01)00101-9

Watts, A. B., & Ten Brink, U. S. (1989). Crustal structure, flexure, and subsidence history of the Hawaiian Islands. *Journal of Geophysical Research*, *94*(B8), 10,473–10,500. https://doi.org/10.1029/JB094iB08p10473

Webster, J. M., Clague, D. A., Riker-Coleman, K., Gallup, C., Braga, J., Cand, P. D., et al. (2004). Drowning of the −150 m reef off Hawaii: A casualty of global meltwater pulse 1A? *Geology*, *32*, 249–252. https://doi.org/10.1130/G20170.1

Webster, J. M., Wallace, L. M., Clague, D. A., & Braga, J. C. (2007). Numerical modeling of the growth and drowning of Hawaiian coral reefs during the last two glacial cycles (0–250 kyr). *Geochemistry, Geophysics, Geosystems*, *8*, Q03011. https://doi.org/10.1029/2006GC001415

Woodroffe, C. D., & Webster, J. M. (2014). Coral reefs and sea-level change. *Marine Geology*, *352*, 248–267. https://doi.org/10.1016/j.margeo.2013.12.006